Brain, Behavior, and Immunity 80 (2019) 777–792

Contents lists available at ScienceDirect

Brain, Behavior, and Immunity

journal homepage: www.elsevier.com/locate/ybrbi

Contribution of microglial reaction to increased nociceptive responses in high-fat-diet (HFD)-induced obesity in male mice

Ya-Jing Liang[a], Shi-Yang Feng[a], Ya-Ping Qi[a], Kai Li[a], Zi-Run Jin[b], Hong-Bo Jing[b], Ling-Yu Liu[b], Jie Cai[b], Guo-Gang Xing[b,c,*], Kai-Yuan Fu[a,c,*]

[a] Center for TMD and Orofacial Pain, Peking University School and Hospital of Stomatology, Beijing 100081, China
[b] Department of Neurobiology, School of Basic Medical Sciences and Neuroscience Research Institute, Peking University, Beijing 100083, China
[c] Key Laboratory for Neuroscience, Ministry of Education/National Health Commission, Peking University, Beijing 100083, China

ARTICLE INFO

Keywords:
High-fat diet
Obesity
Pain hypersensitivity
Microglia
Spinal cord
Inflammation

ABSTRACT

The progressive increase in the prevalence of obesity in the population can result in increased healthcare costs and demands. Recent studies have revealed a positive correlation between pain and obesity, although the underlying mechanisms still remain unknown. Here, we aimed to clarify the role of microglia in altered pain behaviors induced by high-fat diet (HFD) in male mice. We found that C57BL/6CR mice on HFD exhibited enhanced spinal microglial reaction (increased cell number and up-regulated expression of p-p38 and CD16/32), increased tumor necrosis factor-α (TNF-α) mRNA and brain-derived neurotrophic factor (BDNF) protein expression as well as a polarization of spinal microglial toward a pro-inflammatory phenotype. Moreover, we found that using PLX3397 (a selective colony-stimulating factor-1 receptor (CSF1R) kinase inhibitor) to eliminate microglia in HFD-induced obesity mice, inflammation in the spinal cord was rescued, as was abnormal pain hypersensitivity. Intrathecal injection of Mac-1-saporin (a saporin-conjugated anti-mac1 antibody) resulted in a decreased number of microglia and attenuated both mechanical allodynia and thermal hyperalgesia in HFD-fed mice. These results indicate that the pro-inflammatory functions of spinal microglia have a special relevance to abnormal pain hypersensitivity in HFD-induced obesity mice. In conclusion, our data suggest that HFD induces a classical reaction of microglia, characterized by an enhanced phosphorylation of p-38 and increased CD16/32 expression, which may in part contribute to increased nociceptive responses in HFD-induced obesity mice.

1. Introduction

Obesity is a chronic disease and is a growing problem worldwide due to its association with severe disorders (Keane et al., 2013). In the last decade, numerous epidemiological studies have revealed a positive correlation between obesity and chronic pain (Hitt et al., 2007; Marcus, 2004; Stone and Broderick, 2012). Recent studies in animals have demonstrated that obesity further exacerbates pain caused by arthritic conditions (Loredo-Perez et al., 2016), local inflammation of the dorsal root ganglia, complete Freund's adjuvant-induced paw inflammation (Song et al., 2017), and capsaicin-induced orofacial pain (Rossi et al., 2013). However, the mechanisms underlying this association remain unknown.

There are several possible explanations for the positive relationship between obesity and pain. A combination of mechanical-structural, endocrine, and metabolic changes may be potential contributors. Systematic, low-grade chronic inflammation is another popular opinion (Cooper et al., 2017; da Cruz Fernandes et al., 2018; Song et al., 2018). According to this notion, obesity results in a pro-inflammatory state with low-grade, chronic inflammation accompanied by metabolic cells in tissues throughout the body (Gregor and Hotamisligil, 2011). In peripheral tissues, this is orchestrated by immune changes because the resident macrophages, which in healthy condition exhibit alternatively-activated M2-like polarization, switch to classically-activated M1-like polarization. This leads to the release of pro-inflammatory factors and recruitment of circulating monocytes, which further contributes to the pro-inflammatory condition.

Microglia serve as the resident immune cells of the central nervous system (CNS), with functions similar to those of macrophages in peripheral tissues. They further build the first line of defense against

* Corresponding authors at: Department of Neurobiology, School of Basic Medical Sciences and Neuroscience Research Institute, Peking University, 38 Xue-Yuan Road, Hai-Dian District, Beijing 100083, China (G.-G. Xing). Center for TMD and Orofacial Pain, Peking University School and Hospital of Stomatology, No 22 Zhongguancun South Ave, Hai-Dian District, Beijing 100081, China (K.-Y. Fu).
E-mail addresses: ggxing@bjmu.edu.cn (G.-G. Xing), kqkyfu@bjmu.edu.cn (K.-Y. Fu).

https://doi.org/10.1016/j.bbi.2019.05.026
Received 27 October 2018; Received in revised form 11 May 2019; Accepted 16 May 2019
Available online 17 May 2019
0889-1591/

disturbances to local brain homeostasis (Hanisch and Kettenmann, 2007). Studies in rodent models have demonstrated that obesity induces neuroinflammation mediated by increased levels of inflammatory cytokines and microglial reaction within specific brain regions such as hippocampus, hypothalamus, and forebrain regions (de Kloet et al., 2014; Hao et al., 2016; Thaler et al., 2013; Valdearcos et al., 2014; Valdearcos et al., 2015). However, whether such effects could be induced in the spinal cord has not been investigated.

The spinal cord is the first relay station in the process of nociceptive signal transmission from the periphery to the brain. Spinal microglia are activated following injury to the peripheral nerves (Echeverry et al., 2008; Zhang and De Koninck, 2006) and play important roles in the pathogenesis of neuropathic pain and inflammatory pain (Calvo and Bennett, 2012; Li et al., 2010; Zhang et al., 2007). Recent studies have provided strong evidence to show that spinal microglia are not only involved in the genesis of pain but also required for the maintenance of pain hypersensitivity (Echeverry et al., 2017). Microglia are activated by adenosine triphosphate (ATP), colony-stimulating factor-1 (CSF1), chemokines ((C–C motif) ligand 2 (CCL2) and CX3CL1), and proteases, which originate from injured or activated neurons (Guan et al., 2016; Old and Malcangio, 2012; Sawada et al., 2014; Tsuda et al., 2013). In parallel, expression of ATP receptors and CX3CR1 are selectively increased in spinal microglia in response to nerve injury (Grace et al., 2014; Ji et al., 2013). Activation of these receptors typically converges on an intracellular signaling cascade involving the phosphorylation of p38 mitogen-activated protein kinase (MAPK) (McMahon and Malcangio, 2009), which leads to an increased level of tumor necrosis factor-α (TNF-α), interleukin (IL)-1β, IL-18, and brain-derived neurotrophic factor (BDNF), as well as an increased expression of cyclooxygenase (COX) and synthesis of prostaglandin E_2 (Coull et al., 2005; McMahon and Malcangio, 2009). These neuromodulators then fine-tune both excitatory and inhibitory synaptic transmission, which ultimately enhance pain signal transmission to the brain.

Here, we hypothesized that neuroinflammation involving microglial reaction would contribute to increased nociceptive responses in HFD-induced obesity mice. We first validated this hypothesis by investigating the effects of diet-induced obesity on basal nociceptive behaviors, microglial reaction, and the expression of inflammatory cytokines in the spinal cord.

2. Methods

2.1. Animals and treatment

Experiments were carried out in male C57BL/6CR mice (18 to 20 g (g), 3 weeks old) (Vital River Laboratory Animal Technology Co. Ltd, Beijing, P R China), due to recent studies indicated that microglia had an essential role in pain perception in male animals (Rosen et al., 2019; Sorge et al., 2015; Taves et al., 2016). Mice were housed 4 to 5 per cage in a temperature- and humidity- controlled vivarium and on a 12:12-hour light/dark cycle beginning at 07:00. All protocols were approved by the Animal Care and Use Committee of Peking University Health Science Center, who certified that our care and use of animals conformed to national and international guidelines (No. LA2015033).

2.1.1. High-fat diet administration

Mice had *ad libitum* access to food and water. A standard chow diet (CD) and a high-fat diet (HFD) (Research Diets, catalog D12451) were supplied. On a caloric basis, the CD contained 11.5% fat, 20.8% protein, and 67.7% carbohydrate, while the HFD contained 45% fat, 20% protein, and 35% carbohydrate. After 7-day (d) acclimating to the animal facility, mice were randomly divided into age-matched 6 groups (CD group and HFD-fed 1w, 2w, 4w, 6w, and 8w group). For example, mice in the HFD group were fed the diet for 2 weeks (HFD-fed 2w). They received a CD for 6 weeks and then a HFD for 2 weeks, corresponding to a total time of 8 weeks. Following dietary manipulation and pain behavior testing, mice were sacrificed, and blood and spinal dorsal horn samples were collected. Furthermore, gonadal fat pads were immediately removed and weighed on an electronic scale.

2.1.2. Depletion of microglia using pexidartinib (PLX3397)

Pexidartinib (PLX3397, SelleckChem, S7818), a selective colony-stimulating factor-1 receptor (CSF1R) kinase inhibitor, was administered via oral gavage to deplete microglia. In the CNS, PLX3397 has been found to act specifically on microglia, which are the only cell type to express CSF1R under normal conditions (Erblich et al., 2011; Nandi et al., 2012). Mice depleted of microglia exhibit no behavioral or cognitive abnormalities and chronic PLX3397 treatments eliminated tumor-associated macrophages, but had only modest effects on macrophage numbers in other tissues in wild-type mice (Elmore et al., 2014; Mok et al., 2014). PLX3397 was prepared by mixing with 5% dimethylsulfoxide, 45% polyethylene glycol 300, and 50% dd H_2O in sequence, per the manufacturer's instructions. CD-fed 8w and HFD-fed 8w mice were injected once a day over the last week of diet exposure. Behavioral tests were conducted within 10 h, and at day 1, 3, and 5 after drug administration. The concentration of PLX3397 used here (46.25 mg/kilogram (mg/kg) body weight) was based on recent studies (Elmore et al., 2014; Liddelow et al., 2017) and corresponded to a quantity of 290 mg/kg of chow. An equal volume of solution without PLX3397 was used as the vehicle group.

2.1.3. Depletion of spinal microglia using Mac-1-saporin

In order to determine the role of spinal microglia in pain hypersensitivity, we intrathecally administered Mac-1-saporin (Chen et al., 2018; Ferrini et al., 2013; Zhao et al., 2007), a microglia selective toxin (5.6 microgliter (μl)/injection/mouse, 2 μg/μl) at the level of L4-L5 after 8-week feeding course (Ueda et al., 2018; Yao et al., 2016). Vehicle groups received intrathecal injection of same volume of saline. Behavioral tests were conducted at day 1 after Mac-1-saporin treatment.

2.1.4. Determination of biochemical parameters

Levels of total blood cholesterol, triglycerides, and glucose were measured using commercial testing monitors (Accutrend Plus CTL, Roche Diagnostics). After an 8-week altered diet period, animals were fasted for 4 h and blood samples were collected upon sacrifice.

2.2. Pain behavior tests

Behavioral measures of nociception were evaluated at the end of the altered diet period (8 weeks). Mice were habituated to the testing environment daily for at least 2 days prior to testing. Behavioral tests were performed blinded and under constant conditions (23 ± 2 °C; 55 ± 5% humidity) between 09:00 and 12:00 AM in a quiet room.

2.2.1. Response to von Frey filaments

This method was referred to Pogatzki and Raja (Pogatzki and Raja, 2003) and performed to test paw sensitivity to mechanical stimuli. Mice were placed on an elevated plastic mesh floor in a clear Plexiglas chamber (5 × 5 × 8 cm). After a 20 to 30 min (min) acclimation period, withdrawal responses to punctate mechanical stimuli were determined using calibrated von Frey filaments (with 0.07, 0.17, 0.40, 0.60, 1.00, 1.40, and 2.00 g bending forces; North Coast Medical, Atlanta, USA). Each monofilament was applied five times to the plantar aspect of the right hind paw for ~ 1 s (s) with a 10-s interval between stimuli, starting with a force of 0.07 g and continuing in ascending order. A stimulus-related withdrawal of the paw was considered a withdrawal response. The paw withdrawal threshold (PWT) was the force at which withdrawal occurred at least 3 times and 2.0 g was recorded as the PWT if < 3 responses to all filaments occurred.

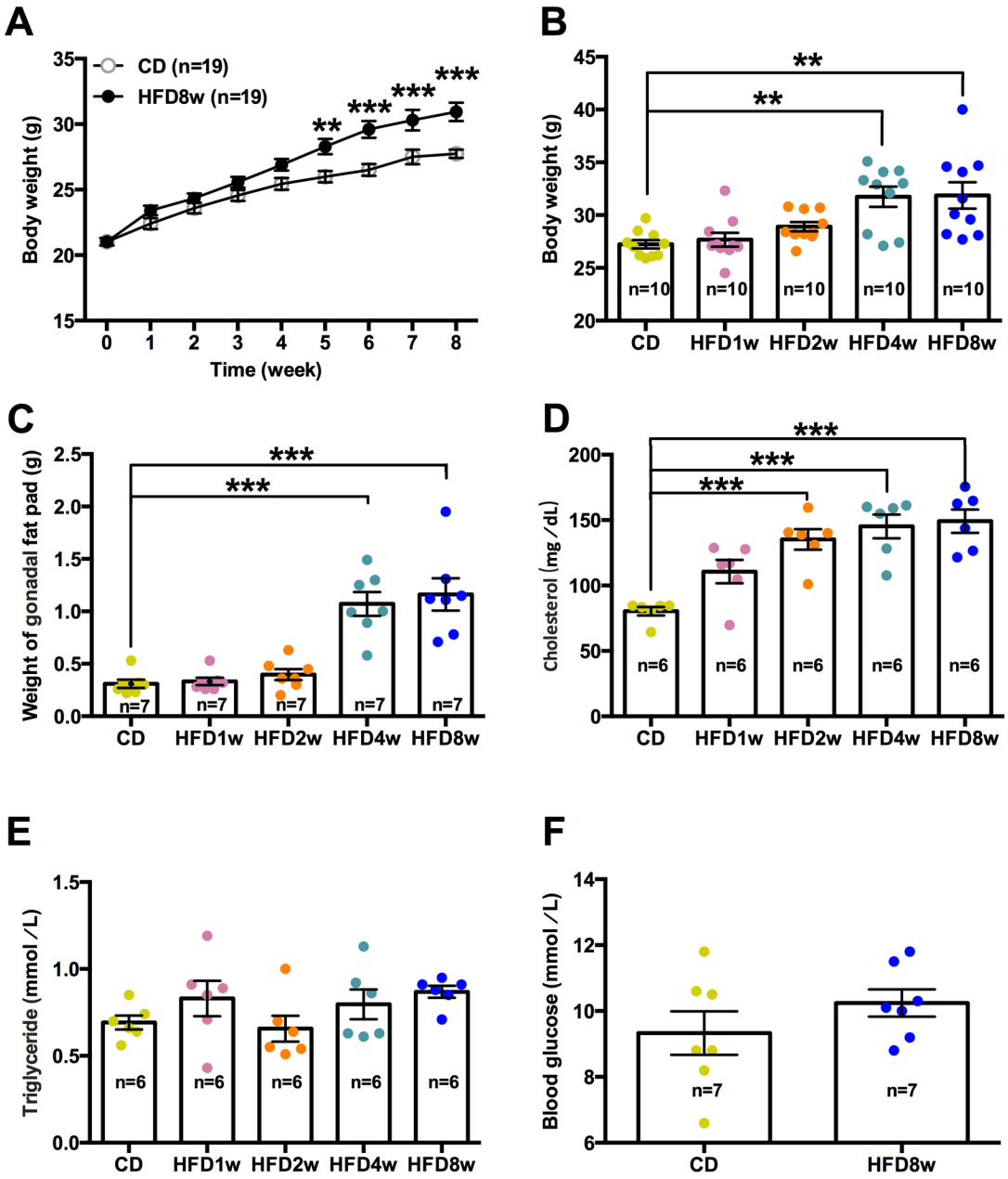

Fig. 1. Effects of high-fat diet (HFD) on body weight, body fat tissue, cholesterol, triglycerides, and blood glucose in mice. (A) Body weight during an 8w-HFD exposure. Note that the body weight is increased after 5 weeks of HFD exposure. Two-way repeated measure ANOVA with Bonferroni's multiple comparisons posttest; n = 19 mice per group. (B) Body weight among CD-fed, HFD-fed 1w, 2w, 4w, and 8w mice. Note the weights of HFD-fed 4w and 8w mice are significantly higher than those of CD-fed mice (n = 10 mice per group). (C) Weights of gonadal fat pads among CD-fed, HFD-fed 1w, 2w, 4w, and 8w mice. The weights of gonadal fat pads are altered in HFD-fed 4w and 8w mice, but are not significantly different among CD-fed, HFD-fed 1w, and HFD-fed 2w groups. (D) Plasma cholesterol among CD-fed, HFD-fed 1w, 2w, 4w, and 8w mice. High-fat diet elevates plasma cholesterol in HFD-fed 2w, 4w and 8w mice compared with CD-fed mice. (E, F) Plasma triglycerides and blood glucose among CD-fed, HFD-fed mice. There is no significant difference for plasma triglycerides and blood glucose among groups. One-way ANOVA with Bonferroni's posttest within groups; $F_{(4,45)} = 7.533$ for body weight data, $F_{(4,30)} = 21.31$ for weight of gonadal fat pad data, $F_{(4,25)} = 13.08$ for cholesterol data, and $F_{(4,25)} = 1.572$ for triglyceride data; n = 6–10 mice per group. Blood glucose was compared by unpaired *t*-test, $t_{12} = 1.17$, $p = 0.26$, n = 7 mice/group. $^{**}p < 0.01$; $^{***}p < 0.001$.

2.2.2. Response to radiant heat stimulation

Paw withdrawal latency (PWL) to heat stimulation was determined in a manner similar to that described previously. After acclimation for 20 to 30 min, a radiant heat source was focused on the middle of right hind paw from underneath the glass. The time required to cause withdrawal of the paw from the stimulus was measured to the nearest 0.1 s (cutoff time 20 s). The results of three trials, 5 to 10 min apart, provided the average PWL.

2.2.3. Rotarod test

Motor coordination was evaluated with two protocols using a rotarod apparatus (Panlab SL, Barcelona, Spain). In the training protocol, the rotation of the rod was set at a constant speed of 4 rpm. In the testing protocol, the rod accelerated from 4 to 40 rpm over a 5 min period, as has been described previously (Galante et al., 2009). All animals were trained for 3 days prior to testing. Animals' latencies (in seconds) to their first fall were recorded with a cut-off time of 300 s. Resulting data represents the mean amount of time each animal stayed

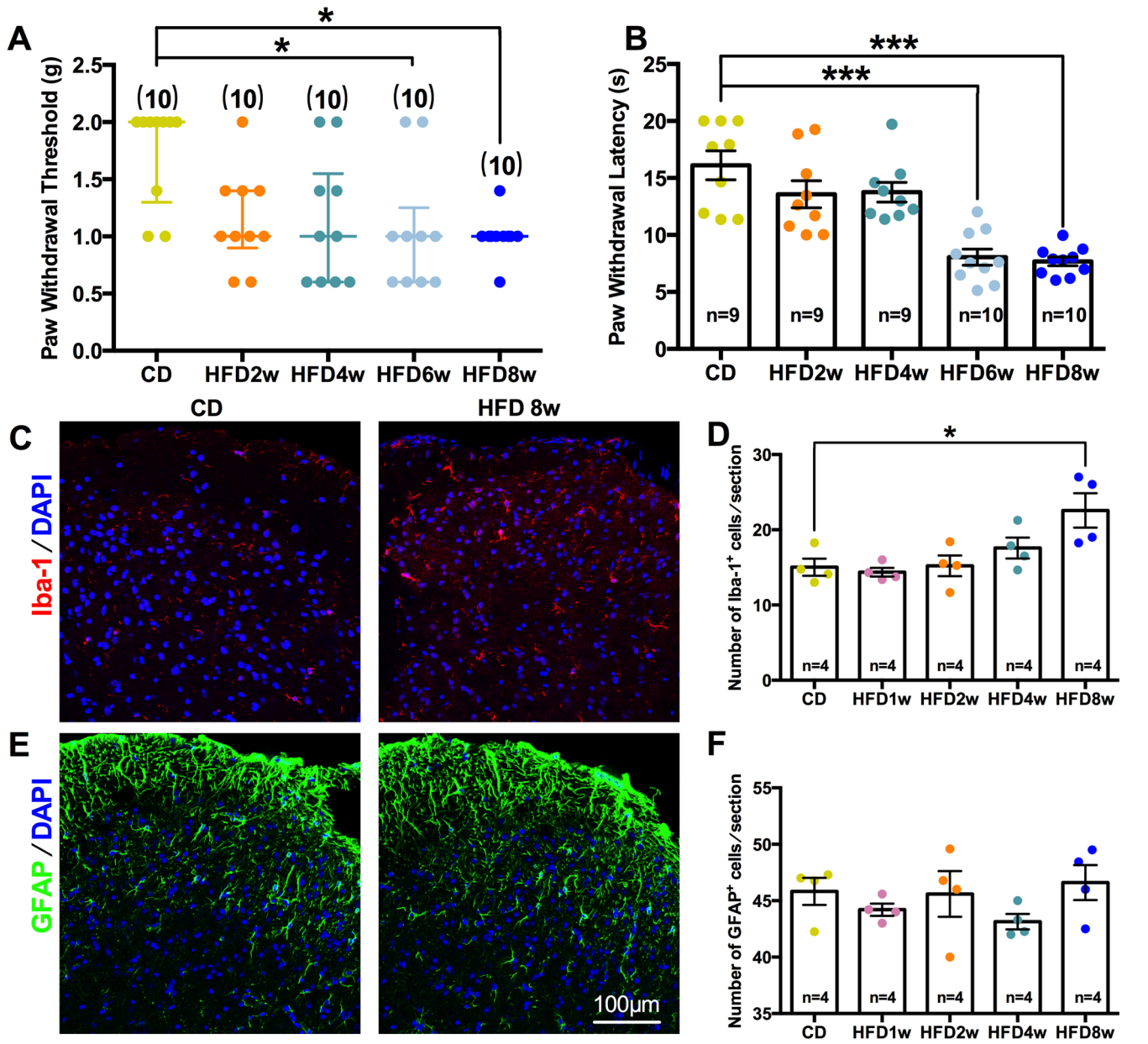

Fig. 2. HFD induces both pain hypersensitivity and increased numbers of Iba-1$^+$ cells in the lumbar spinal dorsal horn. (A) Paw withdrawal thresholds (PWT) of the right hind paw are expressed as medians with first and third quartiles (Two-tailed Dunn's test used to make comparisons following Kruskal-Wallis test. n = 10 mice per group). (B) HFD-fed 6w and 8w mice exhibit a significant decrease in paw withdrawal latency (PWL) (n = 9–10 mice per group). (C-D) Representative examples of IHC and quantitative analyses of Iba-1/DAPI (red/blue) staining in L4-6 spinal dorsal horn. Scale bar: 100 μm. The number of Iba-1$^+$ cells in HFD-fed 8w mice is significantly increased above those in CD-fed mice. (E-F) Representative examples of IHC and quantitative analyses of GFAP/DAPI (green/blue) staining in L4-6 spinal dorsal horn. Scale bar: 100 μm. There is no significant change in GFAP$^+$ cell numbers among CD-fed and HFD-fed mice. One-way ANOVAs with Bonferroni's posttest within groups; $F_{(4,42)} = 17.08$ for PWL data, $F_{(4,15)} = 5.302$ for the number of microglia; $F_{(4,15)} = 1.108$ for the number of astrocytes. Each symbol represents one mouse with at least eight measured sections per mouse, n = 4. *$p < 0.05$; ***$p < 0.001$. (For interpretation of the references to colour in this figure legend, the reader is referred to the web version of this article.)

on the rotarod across 3 trials, with a minimum of 30 min of rest between each trial. The rod was cleaned with 75% ethanol before the next animal was tested.

2.3. Western blot

Mice were deeply anesthetized with 1% sodium pentobarbital and then decapitated. L4-6 spinal cord segments were rapidly removed. The dorsal horn was then dissected using the "open book" method (Zhuang et al., 2005). Briefly, the L4-6 segments were dissected, bisected into left and right pieces along the midline, and then further split into dorsal and ventral horns at the level of the central canal. Dorsal horn tissues were then homogenized in ice-cold RIPA buffer (Cell Signaling Technology) supplemented with 1 mM phenylmethylsulfonyl fluoride, phosphatase inhibitors, and a protease inhibitor cocktail (Sigma-Aldrich). This homogenate was centrifuged at 12,000 g for 10 min at 4 °C. The protein concentration in these tissue lysates was determined via a BCA Protein Assay Kit (Pierce, Rockford, IL). Thirty-milligram aliquots then underwent 12% SDS-PAGE and proteins were transferred electrophoretically to PVDF membranes (Millipore, Bedford, MA). After blocking with 5% nonfat milk in Tris-buffered saline with 0.1% Tween-20 for 1 h at room temperature, the membranes were incubated

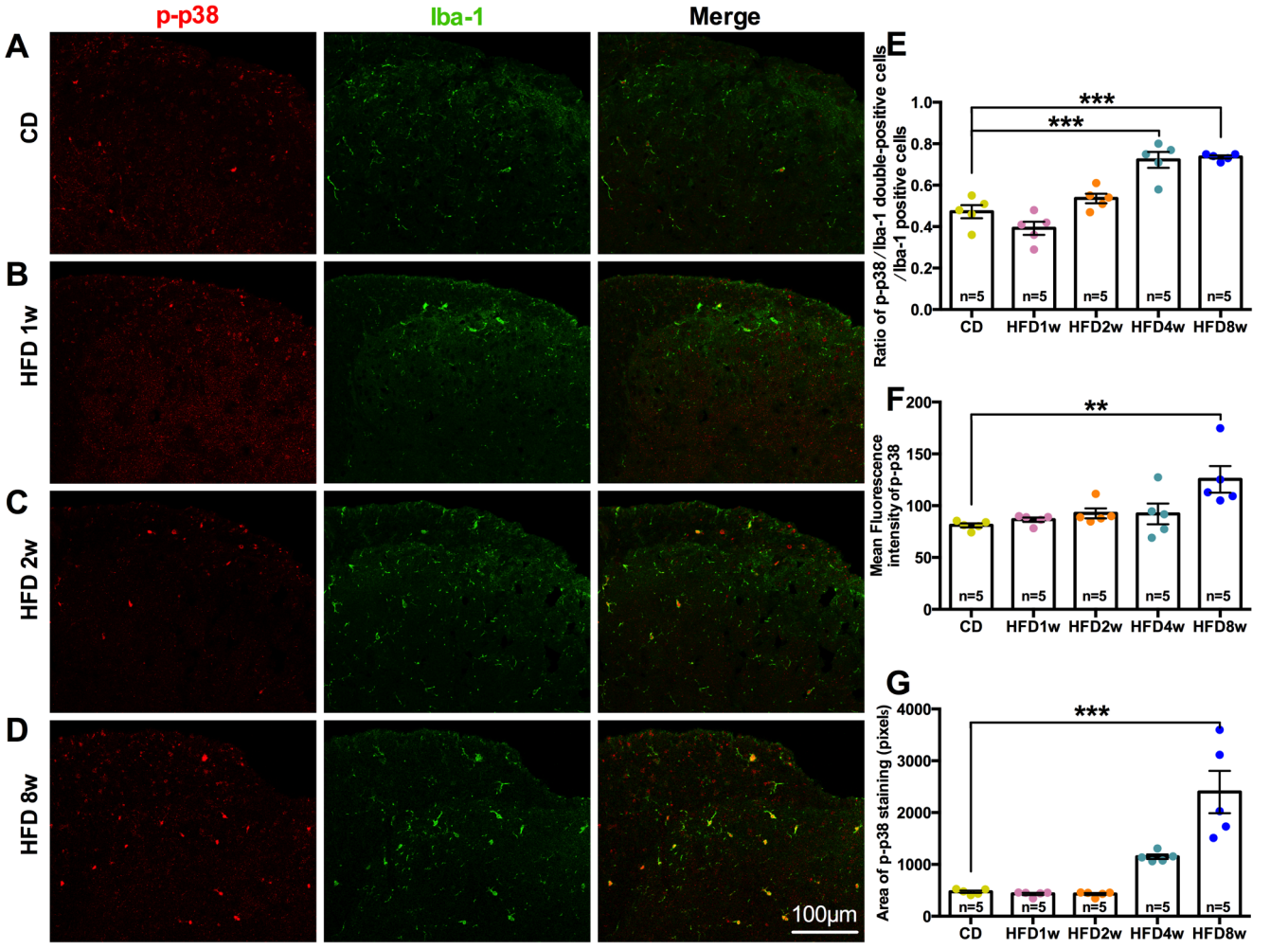

Fig. 3. HFD diet induces p-p38 activation in the lumber spinal cord. (A-D) Representative micrographs of p-p38 and Iba-1 (red/green) immunostaining of tissues in the spinal dorsal horn in CD-fed, HFD-fed 1w, 2w, and 8w mice. Scale bar: 100 μm. (E) Quantitative analysis of the ratio of p-p38/Iba-1 double-positive cells to Iba-1 positive cells shows a progressive increase in HFD-fed 4w and 8w mice. (F-G) Quantitative analyses of p-p38 fluorescence intensity and staining area reveal a significant increase in HFD-fed 8w mice. One-way ANOVA with Bonferroni's posttest within groups; $F_{(4,20)} = 28.42$ for the ratio of p-p38/Iba-1 double-positive cells to Iba-1 positive cells data; $F_{(4,20)} = 5.117$ for p-p38 mean fluorescence intensity data; $F_{(4,20)} = 21.40$ for area of p-p38 staining data. $^{**}p < 0.01$, $^{***}p < 0.001$. Each symbol represents one mouse with at least eight measured sections per mouse, n = 5. (For interpretation of the references to colour in this figure legend, the reader is referred to the web version of this article.)

overnight at 4 °C with antibodies to rabbit anti-phospho-p38 (1:200), rabbit anti-phospho-p44/42 (p-ERK1/2, 1:1000), rabbit anti-phospho-JNK (1:1000), rabbit anti-p38 (1:200), rabbit anti-p44/42 (ERK1/2, 1:1000), rabbit anti-JNK (1:1000; all from Cell Signaling, Beverly, MA), and rabbit anti-BDNF (1:1000, Abcam, Cambridge, MA, USA). After washing, the antibody-protein complexes were probed with HRP-conjugated secondary antibody (1:1000; Jackson). Finally, an enzymatic chemiluminescence Western blot detection kit (Thermo Fisher Scientific, Chelmsford, Massachusetts) was used to assess the expression of target protein. The intensity of immunoblot bands was quantified using Quantity One software (Bio-Rad, Hercules, CA), normalized to the density of the internal control (β-actin), and expressed as fold-changes compared to the control group.

2.4. Immunohistochemistry (IHC) and image analysis

Mice were deeply anesthetized with an overdose of pentobarbital sodium and then perfused transcardially with warm 0.9% saline followed by ice-cold 4% paraformaldehyde in 0.1 M sodium phosphate buffer (pH 7.4). The lumbar spinal cord was removed and placed in the same fixative overnight then transferred to 30% sucrose for cryoprotection. The frozen spinal cord was cut transversely into 30-μm or 50-μm sections on a sliding microtome, collected in PBS, then stored at 4 °C until further use. Standard fluorescence immunohistochemistry protocols were applied with the use of antibodies against selected proteins. Floating sections were washed 3 times in PBS, blocked, and incubated for 24 h at 4 °C with the following primary antibodies: rabbit anti-Iba-1 polyclonal antibody (ionizing calcium-binding adaptor molecule-1 (Iba-1), for microglia, 1:500; Wako, Osaka, Japan, used for double immunofluorescent labels with CD16/32), goat anti-Iba-1 polyclonal antibody (1:200, Abcam, Cambridge, MA, USA, used for double immunofluorescent labels with p-p38), goat anti-CD16/32 polyclonal antibody (Fcγ receptor III/II) (1:200, R&D System, Minneapolis, MN), rabbit anti-phospho-p38 (1:500, Cell Signaling, Beverly, MA), and mouse anti-glial fibrillary acidic protein (GFAP) (1:400, astrocyte marker, Cell Signaling, Beverly, MA). The sections were then washed and incubated for 1 h at room temperature with the secondary antibodies fluorescein (FITC)-conjugated AffiniPure donkey anti-goat, fluorescein (FITC)-conjugated AffiniPure donkey anti-mouse, and Cy3-conjugated AffiniPure donkey anti-rabbit (Jackson Immuno Research, West Grove, PA). Sections were counterstained with 4′, 6-diamidino-2-phenylindole (DAPI) for nuclear labeling. After rinsing

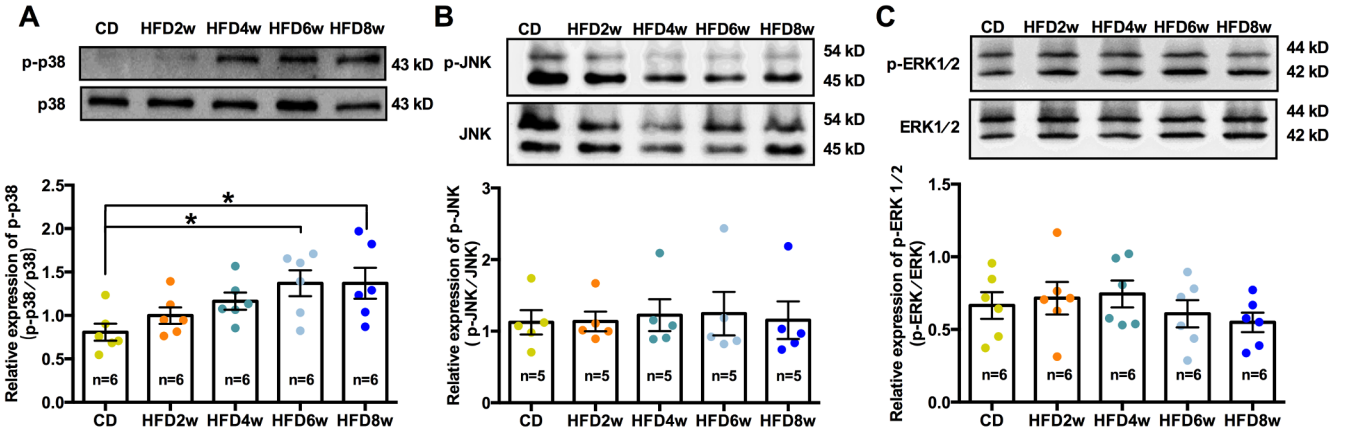

Fig. 4. HFD induces long-lasting microglia reaction with phosphorylated p38 MAPK in the lumbar spinal cord. (A) Western blot of p-p38 expression in lumbar spinal dorsal horn. Upper: representative of Western blot bands; lower: analysis of the relative intensity of p-p38. Note that the expression of p-p38 is significantly increased in HFD-fed 6w and 8w mice compared with CD-fed. Quantification of p-p38 levels is normalized to a control protein, p38. (B, C) Western blot of p-JNK and p-ERK expression in lumbar spinal dorsal horn. Upper: representative of Western blot bands; lower: analysis of the relative intensity of p-JNK and p-ERK. Quantification of p-JNK, p-ERK levels are normalized to JNK and ERK, respectively. Note that the no significant alteration is observed in the expression of p-JNK or p-ERK. One-way ANOVA with Bonferroni's posttest within groups; $F_{(4,25)} = 3.631$ for relative expression of p-p38 data, $F_{(4,20)} = 0.057$ for relative expression of p-JNK data, $F_{(4,25)} = 0.732$ for relative expression of p-ERK data,*$p < 0.05$. n = 5–6 mice per group.

them 3 times in PBST, sections were mounted onto slides and cover-slipped.

Images were acquired on a confocal laser scanning microscope (Leica TCS SP8 STED) at a resolution of 512 × 512 pixels (Leica TCS SP8 STED). Quantitative analyses were performed on images digitized with constant exposure time and gain setting. The staining area of Iba-1$^+$ cells, p-p38, and CD16/32, as well as fluorescent intensity of p-p38 and CD16/32 was quantified using Image Pro Plus (Media Cybernetics, Rockville, MD). The numbers of infiltrated p-p38$^+$/Iba-1$^+$, CD16/32$^+$/Iba-1$^+$, and total Iba-1$^+$ cells were counted manually across each whole section. Ratios of p-p38 and Iba-1 double positive cells to total Iba-1$^+$ cells and ratios of CD16/32 and Iba-1 double positive cells to total Iba-1$^+$ cells were calculated. All measurements were made from 8 to 10 sections per animal with 4–5 animals used per group.

2.5. Semi-automatic quantitative morphometric three-dimensional microglia measurements

50-μm cryosections from spinal cord tissues were stained with anti-Iba-1 (Wako, Osaka, Japan) for 48 h (1:500 dilution at 4 °C) followed by Cy3-conjugated AffiniPure donkey anti-rabbit staining (1:500 overnight at 4 °C). Nuclei were counterstained with DAPI. Imaging was performed on a confocal laser scanning microscope (Leica TCS SP8). Z stacks were obtained with 1.01-μm steps in the z plane. A 512 × 512 pixel resolution was used and analyzed using IMARIS software (Bitplane), as described previously (Erny et al., 2015; Hellwig et al., 2016; Sampson et al., 2016). We selected microglial cells through the spinal dorsal horn randomly. Each individual microglial cell was then reconstructed. Five animals were analyzed per group with five to nine measured cells per mouse. IMARIS based automatic quantification of cell morphometry included process length, number of branch points, number of terminal points, total Sholl intersections, filament area, and volume.

2.6. Real-time quantitative polymerase chain reaction (RT-qPCR)

Gene expression of the inflammatory mediators including TNF-α, IL-6, IL-1β, inducible nitric oxide synthase (iNOS), IL-10, CCL2, and BDNF in the lumbar spinal dorsal horn was measured among groups using real-time PCR. Microglia-specific genes including Iba-1, CX3CR1, CD68, CD206, and spalt-like transcription factor 1 (Sall1) were also compared following treatment with PLX3397 in HFD-fed 8w and CD-fed 8w mice. Total lumbar spinal cord RNA was extracted using TRIzol (Invitrogen, Carlsbad, CA), per the manufacturer's instructions. Total RNA (1 μg) was used as a template for reverse transcription with MMLV reverse transcriptase (Takara, Japan). Template cDNA (1 μL) was amplified by polymerase chain reaction (PCR) with Taq DNA polymerase (Takara) in 25 μL total reaction volume containing 0.5 μM PCR primer as indicated. Quantitative real-time PCR was performed on the ABI 7500 Fast real-time PCR system (Applied Biosysterms, Foster City, CA) with SYBR Premix Ex Taq II (Takara), as previous described (Fang et al., 2015). β-actin was used as an internal control. The final data were normalized to each control group. All primer sequences are listed in Supplementary data, Table S1.

2.7. Data analyses

All data were presented as mean ± SEM, except for the PWTs. Mechanical PWTs were analyzed using nonparametric tests. We used Mann-Whitney tests for two-group comparisons. Kruskal-Wallis test was used for within-group analysis, and a two-tailed Dunn's test was used to make multiple comparisons following the Kruskal-Wallis test. Two-way repeated measure analysis of variance (ANOVA) followed by Bonferroni's *post-hoc* test was used to compare body weights during diet periods. One-way ANOVA following a Bonferroni's *post-hoc* testing and unpaired *t* test was chosen for other data as it is appropriate. $p < 0.05$ was considered to indicate statistical significance. All statistical evaluations were performed using Prism 6 (Graphpad Software, San Diego, CA).

3. Results

3.1. Effects of HFD on body weight, body fat tissue, cholesterol, triglycerides, and blood glucose in mice

As shown in Fig. 1A, the impact of HFD on mouse body weight exhibited after 5 weeks (28.28 ± 0.58 g HFD-fed 5w *vs.* 25.99 ± 0.43 g CD-fed mice, $p = 0.0077$). HFD consumption significantly increased animal body weight over CD-fed animals. The HFD-fed 4w (31.74 ± 0.95 g, $p = 0.0026$) and 8w (31.87 ± 1.25 g, $p = 0.0019$) animals were heavier than CD-fed mice (27.24 ± 0.39 g) (Fig. 1B), while the weights of their gonadal fat pads were also significantly higher ($p < 0.001$, HFD-fed 4w, 8w mice *vs.* CD-fed mice) (Fig. 1C). As compared with the CD-fed mice, the blood cholesterol level was significantly higher in HFD-fed 2w ($p < 0.001$), 4w ($p < 0.001$), and 8w

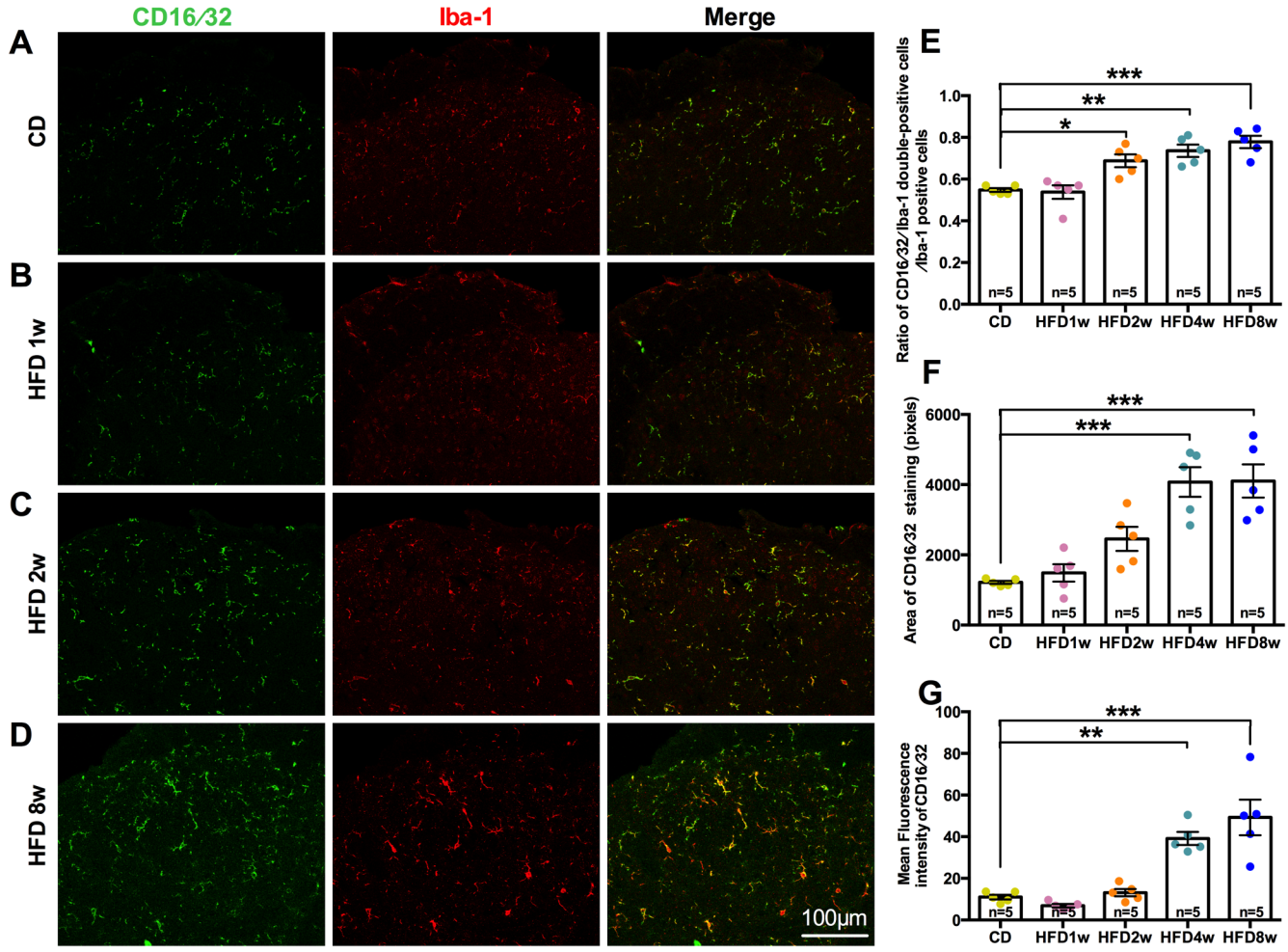

Fig. 5. Activation M1-like microglia phenotype in the lumbar spinal dorsal horn during HFD diet exposure. (A-D) Representative micrographs of CD16/32 and Iba-1 (green/red) immunostaining of tissues in the lumbar spinal dorsal horn in CD-fed, HFD-fed 1w, 2w and 8w mice. Scale bar: 100 μm. (E) Quantitative analysis on the ratio of CD16/32/Iba-1 double-positive cells to Iba-1 positive cells shows a progressive increase, starting at HFD-fed 2w mice and sustaining to HFD-fed 8w mice. (F-G) Quantitative analyses on the CD16/32 staining area and fluorescence intensity showed an obvious increase in HFD-fed 4w and 8w mice. One-way ANOVA with Bonferroni's posttest within groups; $F_{(4,20)} = 15.72$ for the ratio of CD16/32/Iba-1 double-positive cells to Iba-1 positive cells data, $F_{(4,20)} = 16.29$ for area of CD16/32 staining area data, $F_{(4,20)} = 20.57$ for CD16/32 mean fluorescence intensity data. Each symbol represents one mouse with at least eight measured sections per mouse, n = 5 mice per group. $^{*}p < 0.05$; $^{**}p < 0.01$; $^{***}p < 0.001$. (For interpretation of the references to colour in this figure legend, the reader is referred to the web version of this article.)

($p < 0.001$) mice (Fig. 1D). However, HFD consumption did not alter triglyceride or glucose levels (Fig. 1E, F).

3.2. HFD-induced obesity increases nociceptive responses of mice

With respected to the diet-induced obesity and basal pain behaviors, paw withdrawal threshold (PWT) was decreased in the HFD-fed 6w and 8w groups. The median PWT of CD-fed mice was 2.0 g, though this decreased to 1.0 g among HFD-fed 6w ($p = 0.022$) and 8w ($p = 0.045$) animals (Fig. 2A). The paw withdrawal latency (PWL) was 16.11 ± 1.27 s in the CD-fed group, 13.57 ± 1.19 s in the HFD-fed 2w group, and 13.75 ± 0.87 s in the HFD-fed 4w group. HFD-fed 6w (8.05 ± 0.71 s) and 8w (7.69 ± 0.39 s) mice were hypersensitive to heat stimulation when compared to CD-fed mice ($p < 0.001$) (Fig. 2B). These results demonstrated that HFD-fed 6w and 8w mice developed an increased nociceptive response both to mechanical and to thermal stimuli. However, no significant differences in the mean time spent on the rotarod were found between CD-fed and HFD-fed mice (data not shown), indicating that the HFD did not affect the animals' motor function.

3.3. HFD induces long-lasting microglial reaction as indicated by increased phosphorylation of p38 MAPK in the spinal cord

To evaluate the differences in microglia number across all groups, spinal microglia were immunolabeled with Iba-1, which is specifically expressed in microglia in CNS. Quantitative analyses demonstrated that the number of Iba-1^{+} cells in HFD-fed 8w mice was substantially higher than that in CD-fed mice ($p = 0.024$, HFD-fed 8w mice *vs.* CD-fed mice) (Fig. 2C, D). As for astrocytes, HFD-feeding neither altered their morphology nor increased the number of GFAP^{+} cells (Fig. 2E, F).

Few p-p38-immunoreactive cells were found in the spinal cords of CD-fed and HFD-fed 1w mice (Fig. 3A, B). P-p38 protein levels were also nearly undetectable in CD-fed mice by Western blot (Fig. 4A). Further analyses revealed that the ratio of p-p38/Iba-1 double-positive cells to Iba-1 positive cells in HFD-fed 4w and 8w mice were significantly higher than that in CD-fed mice ($p < 0.001$, HFD-fed 4w, and 8w mice *vs.* CD-fed mice) (Fig. 3E). The mean fluorescence intensity of p-p38 was significantly increased in HFD-fed 8w mice ($p < 0.01$, HFD-fed 8w mice *vs.* CD-fed mice), and the area of p-p38 staining was also significantly increased in HFD-fed 8w mice ($p < 0.001$, HFD-fed 8w mice *vs.* CD-fed mice) (Fig. 3F, G). P-p38 protein levels in HFD-fed 6w

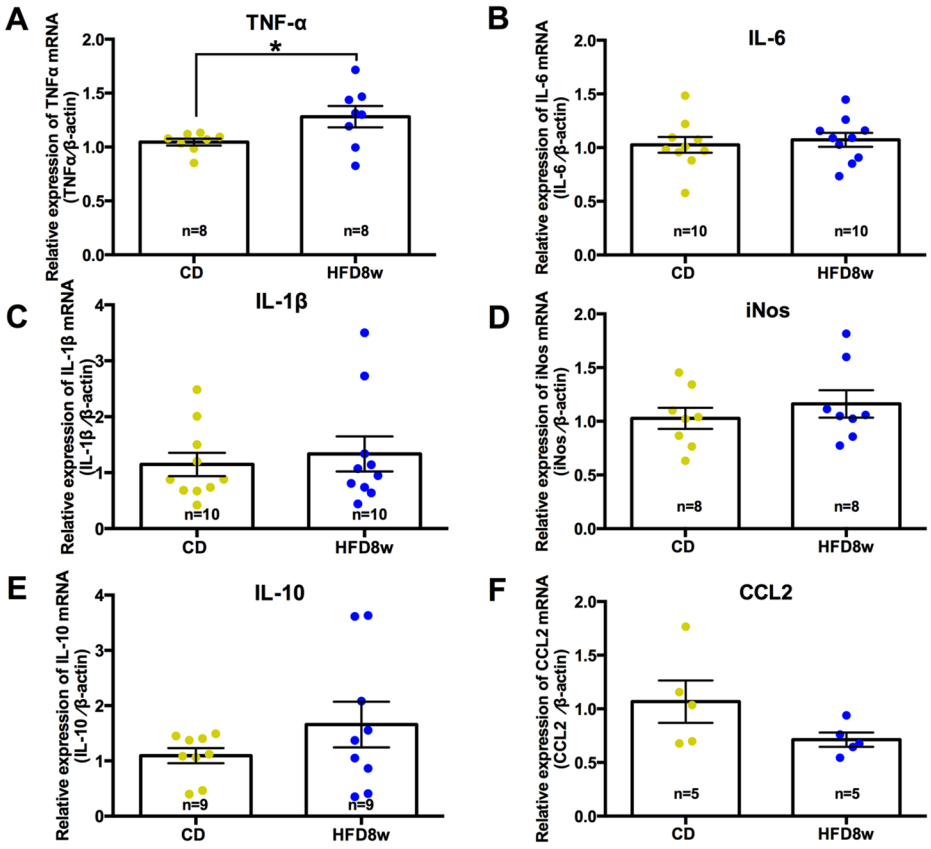

Fig. 6. HFD induces an inflammatory response. (A-F) Relative mRNA levels of TNF-α, IL-6, IL-1β, iNOS, IL-10, and CCL2 in the lumbar spinal dorsal cord in HFD-fed 8w and CD-fed mice. Note that the TNF-α mRNA is increased in HFD-fed 8w mice compared to CD-fed mice. Unpaired *t*-tests between CD-fed and HFD-fed 8w mice, $t_{14} = 2.267$, $p = 0.0397$ for TNF-α mRNA data; $t_{18} = 0.4759$, $p = 0.6399$ for IL-6 mRNA data; $t_{18} = 0.4992$, $p = 0.6237$ for IL-1β mRNA data; $t_{14} = 0.8344$, $p = 0.4181$ for iNOS mRNA data; $t_{16} = 1.296$, $p = 0.2132$ for IL-10 mRNA data; $t_8 = 1.692$, $p = 0.1290$ for CCL2 mRNA data, n = 5–10 mice/group. $^*p < 0.05$.

(~1.70 fold) and HFD-fed 8w (~1.70 fold) mice were higher than those in CD-fed mice ($p = 0.046$, HFD-fed 6w mice *vs.* CD-fed mice; $p = 0.046$, HFD-fed 8w mice *vs.* CD-fed mice) (Fig. 4A). Despite these findings, no significant alterations were found in p-ERK or p-JNK, as determined by Western blot (Fig. 4B, C).

3.4. HFD induces long-lasting microglial reaction as manifested by an increased M1 phenotype in the spinal cord

To determine the functional phenotypes of microglia in HFD-fed mice, spinal microglia were further stained with antibody against CD16/32, a marker of the M1 microglia/macrophage phenotype. A prominent increase in CD16/32 expression in Iba-1$^+$ microglia was observed on the lumbar dorsal horns of HFD-fed 2w and 8w mice, while few CD16/32$^+$ cells were found in CD-fed and HFD-fed 1w mice (Fig. 5A–D). Further analysis demonstrated that the ratio of CD16/32/Iba-1 double-positive cells to Iba-1 positive cells was higher in HFD-fed 2w, 4w, and 8w mice than in CD-fed or HFD-fed 1w mice ($p = 0.019$, HFD-fed 2w mice *vs.* CD-fed mice; $p = 0.0011$, HFD-fed 4w mice *vs.* CD-fed mice; $p < 0.001$, HFD-fed 8w mice *vs.* CD-fed mice) (Fig. 5E). The area of CD16/32 immunostaining was also significantly increased in HFD-fed 4w, and 8w mice ($p < 0.001$, HFD-fed 4w, and 8w mice *vs.* CD-fed mice) (Fig. 5F). Moreover, the mean fluorescence intensity of CD16/32 was significantly increased in HFD-fed 4w and 8w mice ($p = 0.0012$, HFD-fed 4w mice *vs.* CD-fed mice; $p < 0.001$, HFD-fed 8w mice *vs.* CD-fed mice) (Fig. 5G).

3.5. HFD induces an inflammatory response and the release of BDNF in the spinal cord

As the immune cells in the CNS, microglia play significant roles in generating spinal cord inflammatory responses. We detected the expression of several cytokines such as TNF-α, IL-6, IL-1β, iNOS, IL-10, and CCL2 by real-time PCR, among those only TNF-α mRNA level was increased in HFD-fed 8w mice (~1.22 fold) ($p = 0.040$, HFD-fed 8w mice *vs.* CD-fed mice) (Fig. 6A–F). Besides, the BDNF protein, which is recognized as an important molecule in the crosstalk between microglia and neurons in the spinal cord (Coull et al., 2005), was significantly up-regulated in the HFD-fed 8w group (~1.84 fold) ($p = 0.0186$, HFD-fed 8w mice *vs.* CD-fed mice) (Fig. 9A).

3.6. Depletion of microglia and/or suppression microglia gene profile abrogates the HFD-induced pain hypersensitivity, and increased expression of BDNF protein and TNF-α mRNA

To determine whether microglial reaction contributed to increased pain sensitivity following HFD consumption, we applied CSF-1R inhibitor PLX3397 to deplete microglia (Elmore et al., 2014). In the present study, we found a significant decrease in the numbers of Iba-1, p-p38, and CD16/32-positive cells in PLX3397-treated mice as compared to vehicle controls following HFD consumption ($p < 0.001$) (Figs. 7A–H, 8A–F).

To further understand microglia-specific gene changes after PLX3397 treatment, we detected Iba-1, Sall1, CX3CR1, CD68, and CD206 mRNA by real-time PCR. The data showed marked reduction in Iba-1, CX3CR1, CD68, and CD206 mRNA expression in HFD-PLX3397-treated mice compared to HFD-veh-treated mice, indicating substantial microglia depletion (Fig. S1A–E).

Moreover, PLX3397 treatment also inhibited the increased BDNF protein levels (~0.41 fold) ($p = 0.0020$, HFD PLX3397 *vs.* HFD vehicle) and TNF-α mRNA expression induced by 8 weeks of HFD (~0.15 fold) ($p < 0.001$, HFD PLX3397 *vs.* HFD vehicle) (Fig. 9A–B). No significant change was observed in BDNF mRNA expression (Fig. 9C).

We next examined the effects of PLX3397 on pain behaviors following HFD-feeding. The median PWT in HFD-PLX3397 mice was restored from 1.0 g in HFD-vehicle mice to 1.4 g in HFD-PLX3397 mice

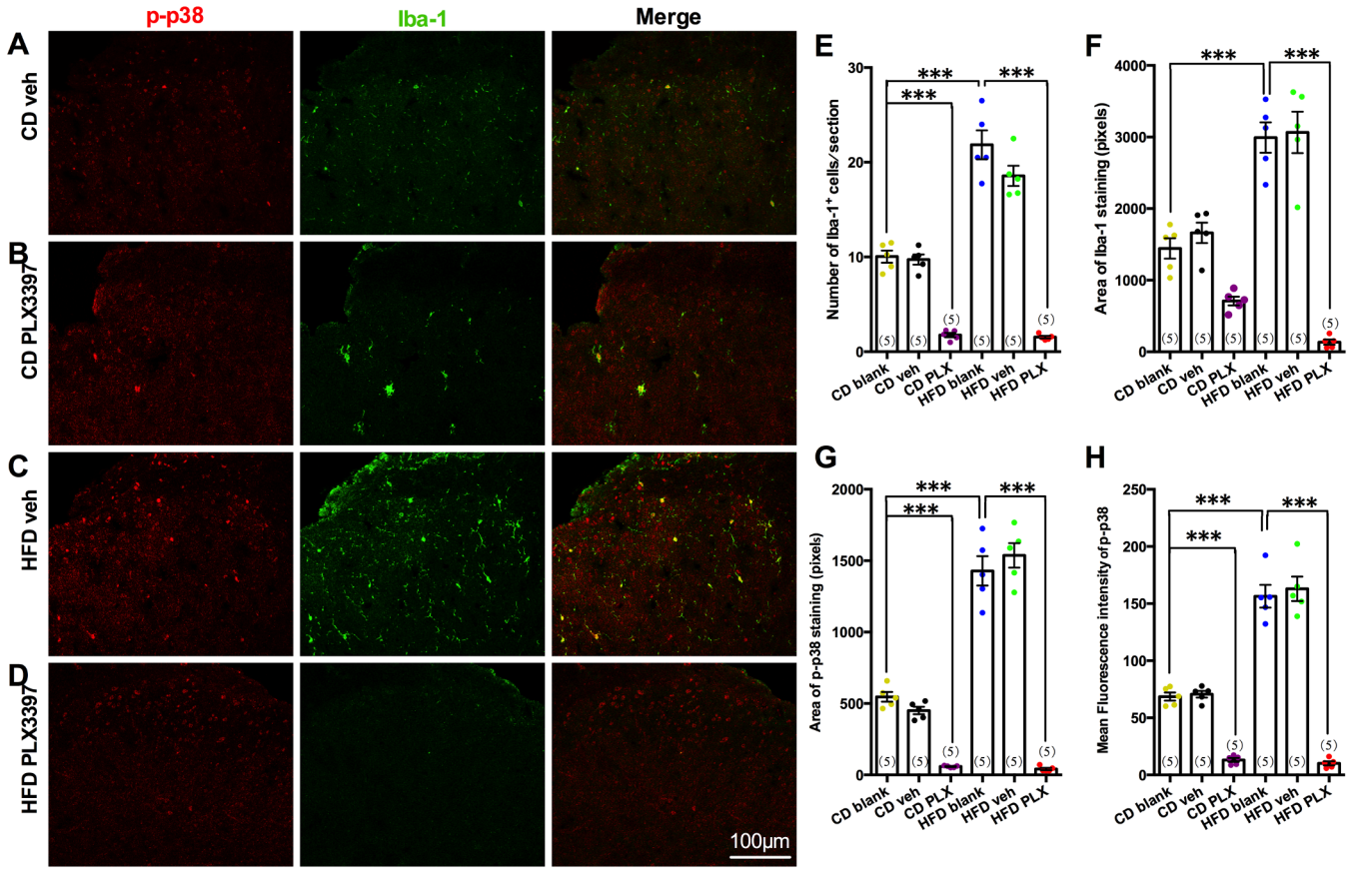

Fig. 7. Impact of microglia depletion on the expression of p-p38 and Iba1 positive cells in the lumbar spinal dorsal horn. (A-D) Representative micrographs of p-p38 and Iba-1 (red/green) immunostaining in the spinal dorsal horn in CD-vehicle, CD-PLX3397, HFD-vehicle, and HFD-PLX3397 mice. Scale bar: 100 μm. (E-F) Quantitative analyses of the number of Iba-1$^+$ cells and Iba-1$^+$ staining area reveal a significant decrease in HFD-PLX3397 mice. (G-H) Quantitative analysis of p-p38 staining area and p-p38 fluorescence intensity reveal a robust decrease in PLX3397-treated mice. One-way ANOVA with Bonferroni's posttest within groups; $F_{(5,24)} = 99.47$ for number of Iba-1$^+$ cells data; $F_{(5,24)} = 48.20$ for area of Iba-1 staining data; $F_{(5,24)} = 130.8$ for area of p-p38 staining data; $F_{(5,24)} = 111.3$ for p-p38 mean fluorescence intensity data. Each symbol represents one mouse with at least eight measured sections per mouse, n = 5. ***$p < 0.001$. (For interpretation of the references to colour in this figure legend, the reader is referred to the web version of this article.)

($p = 0.026$) (Fig. 10A). The PWL was 6.42 ± 0.32 s in the HFD-vehicle group, and was restored to 11.61 ± 0.56 s in HFD-PLX3397 mice ($p < 0.001$) (Fig. 10B). Thus, PLX3397 attenuated the mechanical allodynia and thermal hyperalgesia induced by HFD consumption. Moreover, treatment with PLX3397 did not have any apparent side effects or alteration of animal body weight (Fig. 10C). Also, no statistically significant differences were found among the groups on the rotarod test, indicating that PLX3397 did not impair the motor function of mice (Fig. 10D). Additionally, we examined pain behaviors at more time points after PLX3397 treatment. Mechanical allodynia remained relieved at day 1 after PLX3397 treatment, and returned at day 3 and day 5 after PLX3397 treatment (Fig. S2A). Meanwhile, the thermal hyperalgesia kept alleviated at day 1 and day 3, and returned at day 5 after PLX3397 treatment (Fig. S2B).

3.7. A 3D-reconstructions and semi-automated measurement of cell structures reveals de-ramification of microglia in HFD-fed 8w mice and hyper-ramification of microglia in CD-fed mice in response to PLX3397

As the CNS's immune cells, microglia are activated and undergo phenotypic and morphological alterations upon detection of homeostatic disruptions (Guillemot-Legris and Muccioli, 2017). To further analyze the morphological characteristics for increased Iba-1 in HFD-fed 8w mice, we performed 3D reconstructions of microglia located in the spinal cord and analyzed the following parameters: process length, number of branching points, number of terminal points, total Sholl intersections, filament area, and volume. Semi-automatic quantitative morphometric 3D measurements of microglia revealed significantly shorter processes and decreased total Sholl intersections, and decreased filament area in HFD-fed 8w mice. These features were indicative of de-ramification morphology (Fig. 11A–B, E; Supplementary data, 3D Neuroimaging Data 1 and 2) ($p = 0.0108$ for process length; $p = 0.0155$, for total Sholl intersections; $p = 0.0205$, for filament area; HFD-fed 8w mice *vs.* CD-fed mice).

Morphological analyses for the microglia that survived after PLX3397 administration in CD-fed mice exhibited increased numbers of branch points, terminal points, and total Sholl intersections but no significant changes in process length, filament area, or volume. These cells had structures that were more complicated, a hyper-ramification morphology typically associated with a more immature phenotype (Erny et al., 2015), while the surviving microglia in HFD-PLX3397 mice showed a similar morphology with HFD8w mice. (Fig. 11A, C, D and E; Supplementary data, 3D Neuroimaging Data 1, 3 and 4).

3.8. Intrathecal injection of Mac-1-saporin in the spinal cord depletes microglia and attenuates both mechanical allodynia and thermal hyperalgesia in HFD-fed mice

To determine whether spinal microglia are responsible for HFD-induced pain sensitivity, we depleted spinal microglia by intrathecal injection of Mac-1-saporin (Chen et al., 2018; Ferrini et al., 2013; Ueda et al., 2018; Zhao et al., 2007), a microglia selective toxin which could

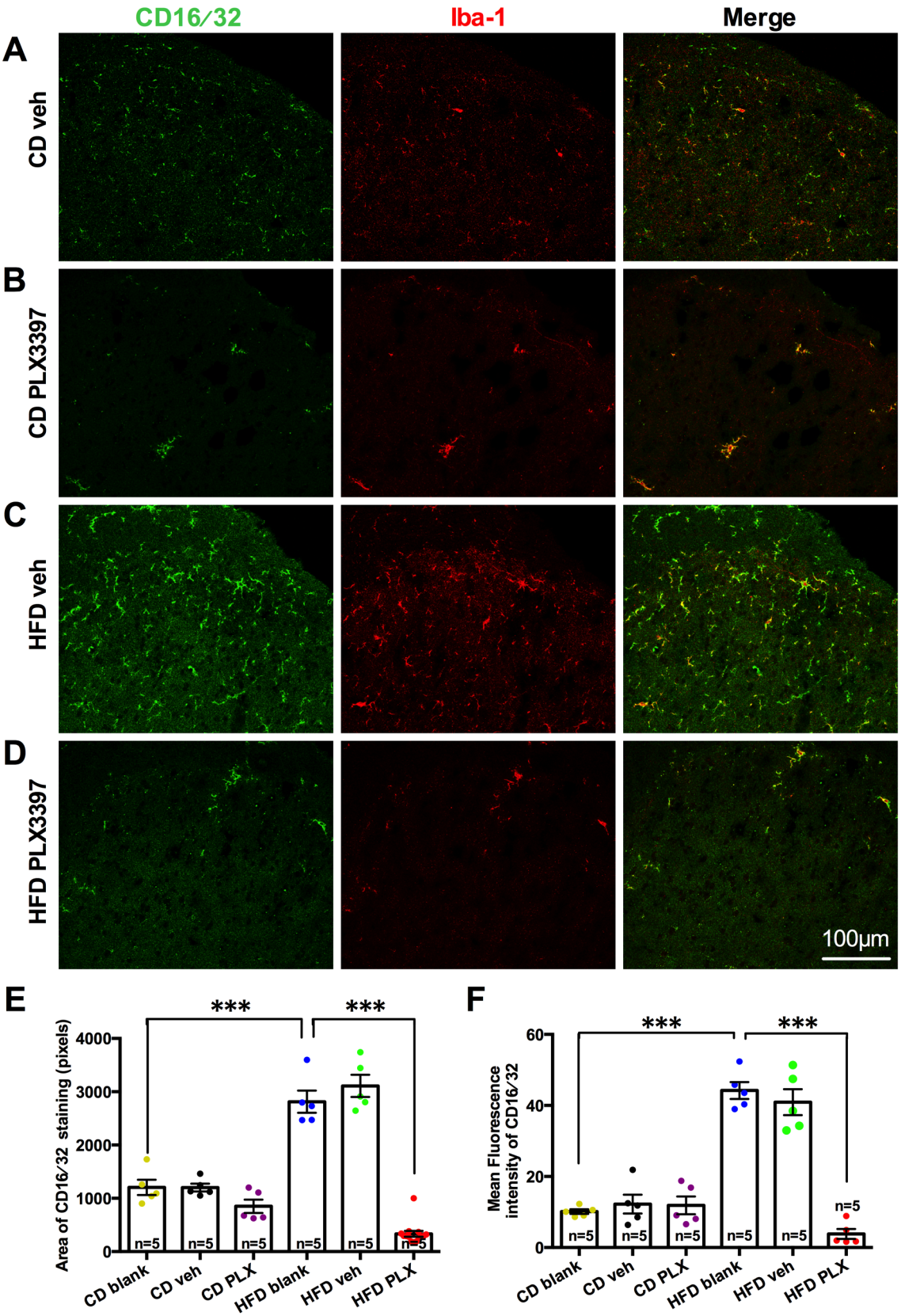

Fig. 8. Presence of M1-like microglia in the lumber spinal cord following 7-day PLX3397 administration in HFD-fed 8w mice. (A-D) Representative micrographs of CD16/32 and Iba-1 (green/red) immunostaining in the spinal dorsal horn in CD-vehicle, CD-PLX3397, HFD-vehicle and HFD-PLX3397 mice. Scale bar: 100 μm. (E-F) CD16/32 staining area and CD16/32 fluorescent intensity are substantially decreased in HFD-fed mice that received PLX3397. One-way ANOVA with Bonferroni's within-group posttest; $F_{(5,24)} = 60.18$ for area of CD16/32 staining intensity data, $F_{(5,24)} = 52.48$ for CD16/32 mean fluorescence intensity. Each symbol represents one mouse with at least eight measured sections per mouse, n = 5. ***$p < 0.001$. (For interpretation of the references to colour in this figure legend, the reader is referred to the web version of this article.)

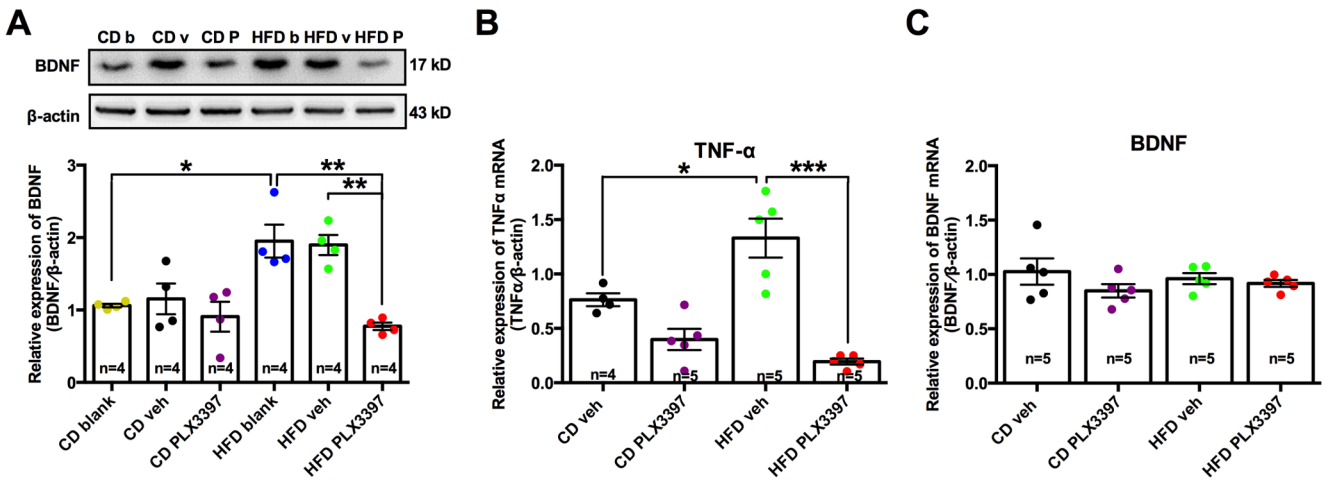

Fig. 9. PLX3397 inhibits the HFD-induced enhancement of spinal BDNF protein and TNF-α mRNA expression. (A) Western blot of BDNF in lumbar spinal dorsal horn. Upper: representative of Western blot bands; lower: analysis of the relative intensity of BDNF. β-actin is used as an internal control. Note that the enhancement of BDNF induced by 8w-HFD exposure is significantly inhibited by PLX3397 treatment. (B-C) Relative expression of TNF-α and BDNF mRNA levels in the lumbar spinal dorsal cord. Expression of TNF-α mRNA is decreased following treatment with PLX3397 and no significant change is observed in BDNF mRNA following PLX3397 treatment. One-way ANOVA with Bonferroni's posttest within groups; $F_{(5,18)} = 9.543$ for BDNF protein data, $F_{(3,15)} = 20.85$ for TNF-α mRNA data, $F_{(3,16)} = 1.014$ for BDNF mRNA data. n = 4–5 mice/group. $^{*}p < 0.05$; $^{**}p < 0.01$; $^{***}p < 0.001$.

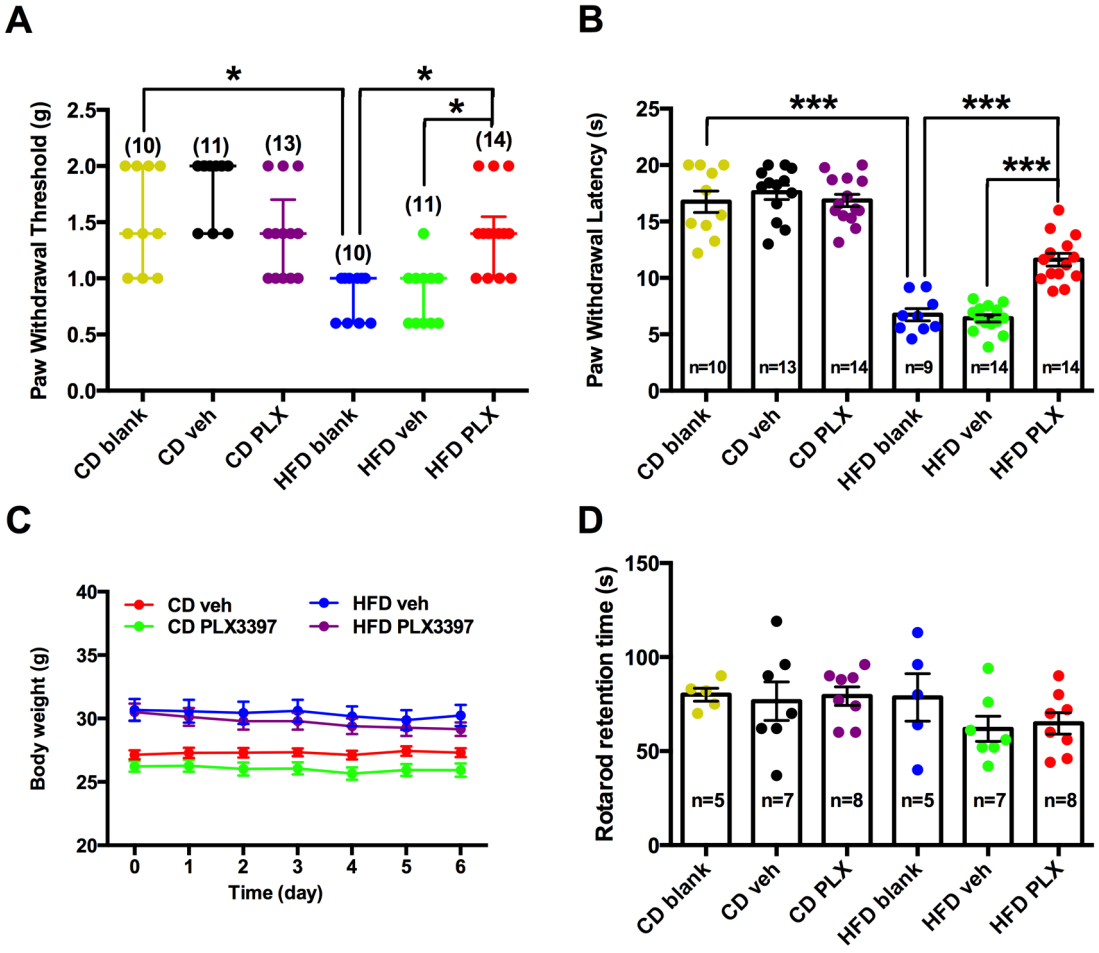

Fig. 10. Depletion of microglia attenuates mechanical allodynia and thermal hyperalgesia in HFD-fed mice. (A-B) Mechanical allodynia and thermal hyperalgesia are reversed by PLX3397 administration. (C) Body weight during PLX3397 treatment in CD-fed and HFD-fed mice. Note the body weight is not altered by PLX3397 administration (two-way repeated measure ANOVA with Bonferroni's multiple comparisons posttest; n = 12 mice per group). (D) Rotarod retention time in the Rotarod test. No significant difference in the mean time spent is observed among different diet groups or PLX3397-treated groups. Results of von Frey tests are expressed a median with first and third quartiles. PWTs to von Frey filaments are analyzed using nonparametric test. Two-tailed Dunn's test is performed to make these comparisons following Kruskal-Wallis test. One-way ANOVA followed by Bonferroni's posttest within groups; $F_{(5,68)} = 73.90$ for PWL data. n = 9–14 mice per group; $F_{(5,34)} = 1.173$ for rotarod retention time data, n = 5–8 mice per group; $^{*}p < 0.05$; $^{***}p < 0.001$.

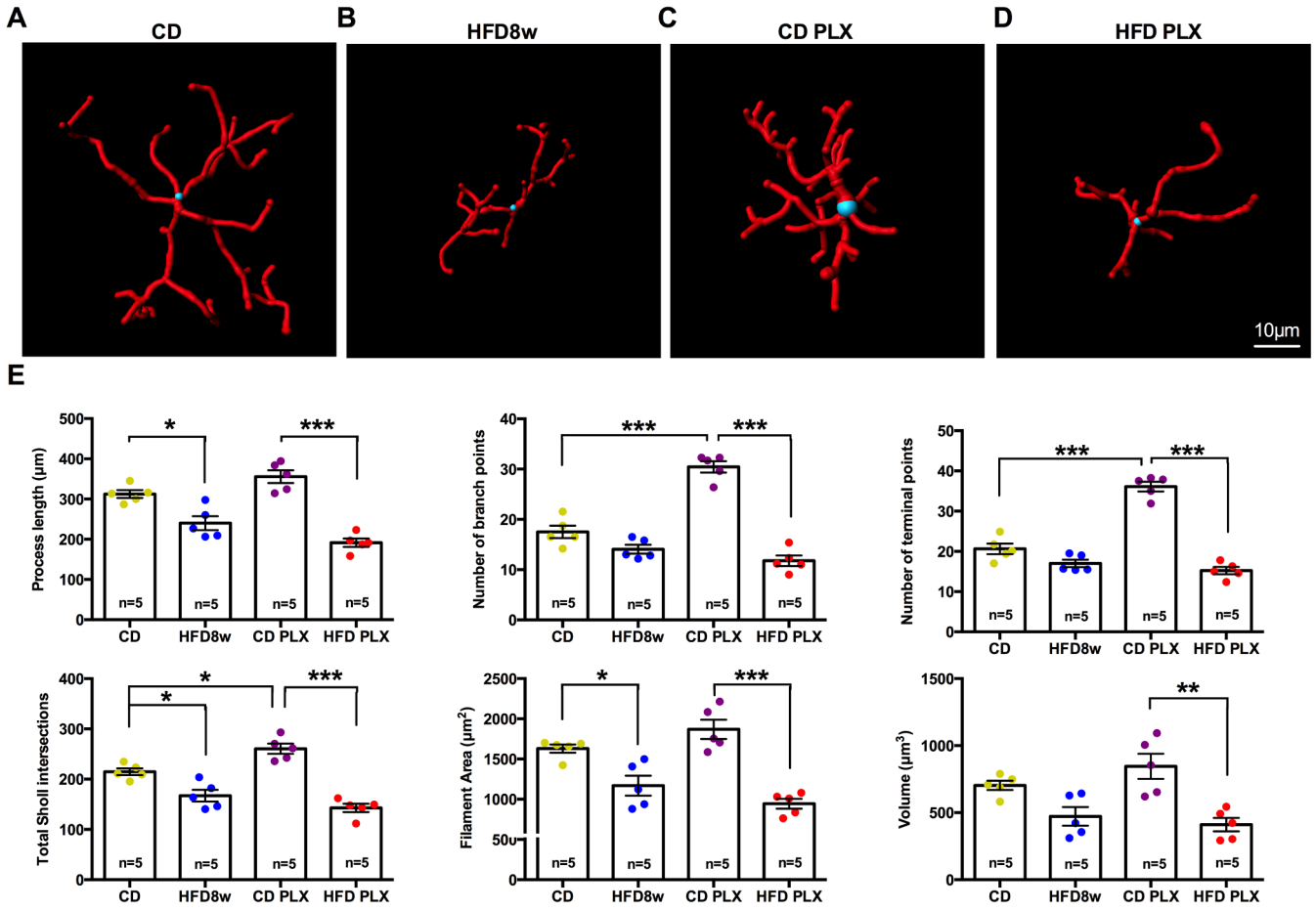

Fig. 11. 3D-reconstructions and IMARIS-based automatic quantifications of spinal Iba-1$^+$ microglia morphometry. (A) Resident spinal cord microglia exhibits typical ramified morphologies, with long, finely branched processes in CD-fed mice. (B) Microglia are switched to de-ramification with fewer and shorter processes (a de-ramified morphology) in HFD-fed 8w mice. (C) Surviving microglia from CD-fed mice treated with PLX3397 exhibits hyper-ramification with increased branching. (D) Surviving microglia in HFD-fed 8w treated with PLX3397 also exhibit a de-ramified morphology. (E) Imaris-based automatic quantification of cell morphometry among spinal microglia in CD-fed mice, HFD-fed 8w mice, CD-fed mice treated with PLX3397 and HFD-fed 8w mice treated with PLX3397. Each symbol represents one mouse. Five animals are analyzed per group with 5–9 measured cells per animal. One-way ANOVA with Bonferroni's posttest within groups; $F_{(3,16)} = 28.67$ for process length, $F_{(3,16)} = 59.31$ number of branch points, $F_{(3,16)} = 75.08$ for number of terminal points, $F_{(3,16)} = 30.64$ for total sholl intersections, $F_{(3,16)} = 19.79$ for area data and $F_{(3,16)} = 9.478$ for volume. $^*p < 0.05$; $^{**}p < 0.01$; $^{***}p < 0.001$. Scale bar: 10 μm.

deplete 50% spinal microglia 1 day after injection (Yao et al., 2016). Compared to HFD8w mice that received vehicle treatment, one day after intrathecal injection of Mac-1-saporin, the number of Iba-1 positive cells and Iba-1 staining area were strikingly decreased in spinal dorsal horn ($p = 0.0037$ for number and $p = 0.0046$ for area) (Fig. 12A–D). Moreover, the area of CD16/32 staining and the mean fluorescence intensity of CD16/32 was also significantly decreased following Mac-1-saporin treatment ($p = 0.0222$ for area and $p = 0.0222$ for mean fluorescence intensity) (Fig. 12A, B, E, F). Measuring pain behaviors demonstrated that targeting spinal microglia with Mac-1-saporin attenuated both mechanical allodynia ($p < 0.001$) and thermal hyperalgesia ($p = 0.0015$) induced by HFD (Fig. 12G–H), while Mac-1-saporin did not impair the animals' motor function (Fig. 12I).

4. Discussion

The most significant findings in the present study are as follows: 1) HFD (45% calories from fat) increased nociceptive responses to both mechanical and thermal stimuli in mice; 2) HFD induced long-lasting microglial reaction in the spinal cord, characterized by up-regulation of p-p38 and CD16/32 and increased levels of the pro-inflammatory cytokine TNF-α mRNA as well as the BDNF protein; 3) microglial depletion ameliorated the pain hypersensitivity and increased expression of TNF-α mRNA and BDNF protein in the spinal cords in HFD-fed mice. Collectively, these results indicate that inflammatory responses associated with spinal microglial reaction contribute to exacerbated pain sensitivity induced by HFD feeding.

4.1. HFD-derived neuroinflammation is a risk factor for chronic pain

Several epidemiological studies have revealed that obesity/body mass index (BMI) has a strong, dose-dependent correlation with pain in the general population (Heim et al., 2008; McCarthy et al., 2009; Narouze and Souzdalnitski, 2015; Paulis et al., 2014; Smuck et al., 2014; Stone and Broderick, 2012). However, the mechanisms underlying chronic pain in obese populations are not fully understood. In a large-scale study in Norway, both BMI and inflammatory cytokine levels are found positively associated with pain severity (Sibille et al., 2016). Moreover, levels of C-reactive protein have been shown to be related to cold sensitivity (Schistad et al., 2017). Collectively, these results suggest that low-grade, chronic inflammation across the whole body serves as a risk factor for pain hypersensitivity. More recently, obesity-derived neuroinflammation has been found to affect brain structures and also be associated with an increased occurrence of CNS disorders such as depression and impaired cognitive function (Guillemot-Legris and Muccioli, 2017).

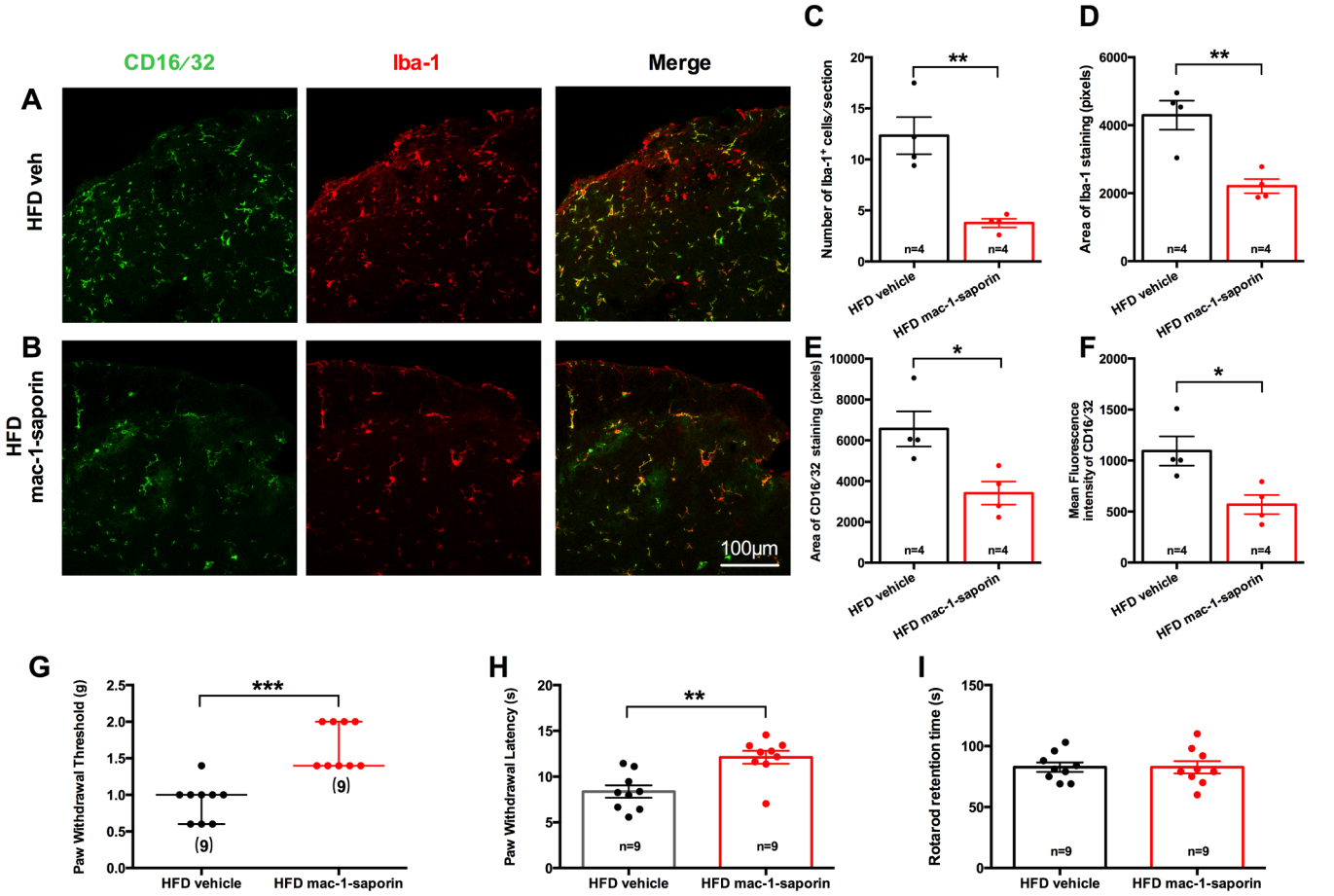

Fig. 12. Intrathecal injection of Mac-1-saporin in the spinal cord decreases microglia and attenuates both mechanical allodynia and thermal hyperalgesia in HFD-fed mice. (A-B) Representative micrographs of CD16/32 and Iba-1 (green/red) immunostaining in the spinal dorsal horn in HFD-vehicle and HFD-mac-1-saporin mice. Scale bar: 100 μm. (C-D) Quantitative analyses of the number of Iba-1$^+$ cells and Iba-1$^+$ staining area reveal a significant decrease in mac-1-saporin-treated mice. (E-F) CD16/32 staining area and CD16/32 fluorescent intensity are substantially decreased in HFD-fed mice that received mac-1-saporin. (G) Mechanical allodynia is rescued at 1 day after mac-1-saporin treatment. Results of von Frey tests are expressed a median with first and third quartiles. PWTs to von Frey filaments are analyzed using nonparametric test (Mann-Whitney test). (H) Thermal hyperalgesia is attenuated at 1 day mac-1-saporin treatment. (I) Rotarod retention time in the Rotarod test. Unpaired *t*-tests between HFD-veh and HFD-mac-1-saporin 8w mice, $t_6 = 4.6$, $p = 0.0037$ for number of Iba-1$^+$ cells data; $t_6 = 4.4$, $p = 0.0046$ for area of Iba-1 staining data; $t_6 = 3.1$, $p = 0.0222$ for area of CD16/32 staining data; $t_6 = 3.1$, $p = 0.0222$ for CD16/32 mean fluorescence intensity data, 7–11 sections/mouse, 4 mice/group; $t_{16} = 3.8$, $p = 0.0015$ for PWL data, $t_{16} = 0.0$, $p > 0.9999$ for rotarod retention time data. Each symbol represents one mouse, n = 4–9. $^*p < 0.05$; $^{**}p < 0.01$; $^{***}p < 0.001$. (For interpretation of the references to colour in this figure legend, the reader is referred to the web version of this article.)

Whether and how inflammatory conditions in the spinal cord contribute to enhanced pain sensitivity in obese patients remains unclear. Several studies have reported that HFD increases nociceptive responses in intact rodents (Cooper et al., 2018; Cooper et al., 2017), exacerbates pain-like behaviors in arthritis (Loredo-Perez et al., 2016) and capsaicin-induced facial pain (Rossi et al., 2016) animal models, and prolongs post-operative pain (Guillemot-Legris et al., 2018; Song et al., 2018). Interestingly, a recent study revealed that different responses to HFD were observed in two substrains of C57BL/6 mice from Jackson laboratories (C57BL/6J and C57BL/6NIH mice) and C57BL/6 mice from Charles Rivers (C57BL/6CR). The C57BL/6CR mice had the highest weights and fat mass of the three substrains and were the only strain to develop significant mechanical pain sensitivity over the course of an 8w HFD protocol. Conversely, C57BL/6J mice were protected from mechanical pain sensitivity due to increased physical activity compared to the other two substrains (Cooper et al., 2018).

In the present study, we observed that C57BL/6CR mice exhibited enhanced nociceptive responses to both mechanical and thermal stimuli after 6w HFD. We also found that the spinal cord was in an inflammatory state, induced by the consumption of HFD, which was characterized by spinal microglial reaction with increased M1 microglia/macrophage phenotype expression and increased TNF-α mRNA and BDNF protein.

4.2. Microglia mediates pro-inflammation in the spinal cord after HFD consumption

As immunes cells, microglia can become activated and undergo phenotypic and morphological changes when homeostatic disruption is detected (Guillemot-Legris and Muccioli, 2017). Specifically, activated microglia participate in a number of physiological and pathological functions such as phagocytosis and cytokine release (Kettenmann et al., 2011) and display enhanced expression of OX-42 (CD11b), p-p38 MAPK, and Fc γ receptors (CD16/32) (Goings et al., 2006; Ji and Suter, 2007). Microglia have been reported to exhibit at least two distinct activation patterns like peripheral macrophages (Cherry et al., 2014; Colton, 2009; Hu et al., 2012; Wang et al., 2014), but the assertion of this opinion has not been established (Ransohoff, 2016). The activated state, the M1 phenotype, is typified by a classical pro-inflammatory response for the production of inflammatory cytokines and reactive oxygen species, antigen presentation, and the removal of pathogens. The expression of M1 marker proteins such as CD16/32 and CD86, as well as major histocompatibility complex II (MHC II), is up-regulated to allow for antigen presentation and crosstalk with other cells (Taylor

et al., 2005). The present study found that HFD-induced spinal microglia exhibit an M1 phenotype characterized by the up-regulation of CD16/32 and production of pro-inflammatory cytokines.

The impact of obesity on microglia has largely been underexplored. Bioactive fatty acids issued from metabolism of nutrients can cross the blood brain barrier to reach the CNS and appear to be direct modulators of microglial activity, triggering/inhibiting inflammatory processes (Nadjar et al., 2017). Recent studies have revealed that excessive dietary SFA consumption specifically activates microglia in the mediobasal hypothalamus, which is mirrored by hypothalamic SFA (especially long-chain SFAs) accumulation. It has also been proposed that the inhibition of pro-inflammatory pathways in microglia is sufficient to protect against diet-induced hypothalamic inflammation and obesity (Valdearcos et al., 2017; Valdearcos et al., 2014). Treating cultured macrophages with long-chain saturated FAs, but not unsaturated species, elicits an inflammatory response reminiscent of what occurs under conditions of dietary excess (Kennedy et al., 2009). BV-2 cells, an immortalized microglial cell line, and primary microglia are also activated by SFA via a TLR4-dependent NF-κB pathway, leading to increased levels of pro-inflammatory cytokines and reactive oxygen species (Button et al., 2014; Wang et al., 2012). Furthermore, FA-activated BV-2 cell culture medium has been shown to be cytotoxic to neurons (Wang et al., 2012).

4.3. Reaction of microglia in the spinal cord is required for increased pain sensitivity in HFD-fed mice

Pro-inflammatory cytokines released by microglia, which have been implicated in mediating glia-neuron interaction, play a critical role in central sensitization and pain hypersensitivity (Goings et al., 2006; Kawasaki et al., 2008; Zhang et al., 2015). Indeed, several lines of evidence have revealed that increased plasma and muscle levels of TNF-α occur in both obese patients and rodents (Cawthorn and Sethi, 2008; Plomgaard et al., 2007; Valerio et al., 2006), suggesting that TNF-α plays a critical role in obesity (Cawthorn and Sethi, 2008; Schreyer et al., 1998; Tzanavari et al., 2010). Microglia p38 activation results in increased synthesis of proinflammatory cytokines, such as TNF-α in male mice (Ji and Suter, 2007). In the present study, we measured several pro-inflammatory cytokines, and only TNF-α mRNA was found to be increased. In addition, an elevated level of BDNF protein was found in the spinal cord of HFD-fed mice. As a member of the neurotrophin family, BDNF can also be released in the spinal cord by activated microglia (Beggs et al., 2012; Coull et al., 2005) and serves as a prerequisite for pain hypersensitivity under abnormal conditions (Echeverry et al., 2017). Activation of p38 in microglia is also implicated in BDNF synthesis and release (Trang et al., 2012; Trang et al., 2009). Therefore, microglia-derived signaling molecules such as BDNF may be key molecules underlying the HFD-induced pain hypersensitivity.

To further explore the involvement of microglial reaction in HFD-induced pain hypersensitivity, microglia in the present study were depleted by 7 days PLX3397 administration. Previous work has revealed that treatment with PLX3397 in mice induces a robust, time-dependent reduction in microglia number, with a 50% reduction by day 3 of treatment and the elimination of most microglia after 7 days of PLX3397 application. PLX3397 treatment did not, however, affect brain volume, cognition, or motor function (Elmore et al., 2014). We observed here that depletions of microglia attenuated pain hypersensitivity in HFD-fed mice, inhibited TNF-α mRNA expression, and reduced BDNF release in the spinal cord. Moreover, we depleted microglia by intrathecal injection of Mac-1-saporin in HFD-fed mice. We found that depletion of microglia in the spinal cord restored pain hypersensitivity. So we suggest that spinal microglia reaction at least in part contributes to the exacerbated pain hypersensitivity induced by a high-fat diet, but we can not rule out the influence of brain microglia.

4.4. HFD changes the 3D morphology of spinal microglia

In general, microglial cell morphology changes from ramified to amoeboid when reacted in response to peripheral stimulation (de-ramification). In the present study, 3D reconstructions and automated measurements of microglia revealed a de-ramification of spinal microglia in mice exposed to 8w HFD, indicating an occurrence of reacted microglia phenotype. Surprisingly, microglia from CD-fed 8w mice treated with PLX3397 exhibited hyper-ramification and a greater complexity of morphology, as characterized by increased numbers of branch points, terminal points, and total Sholl intersections. However, this hyper-ramification was not found in HFD-fed 8w mice treated with PLX3397. Very little is known about the factors that initiate hyper-ramification or the *in vivo* function(s) of hyper-ramified microglia (Hellwig et al., 2013). Additionally, the concept of microglia "activation" has been challenged by several lines of evidence; it is becoming increasingly clear that microglia in healthy systems can also be active, and that with pathological conditions they acquire disease-specific phenotypes (Hanisch, 2013; Hellwig et al., 2013; London et al., 2013). The 3D reconstructions and semi-automated measurements of cell structures done in the present study revealed de-ramification of spinal microglia in HFD-fed 8w mice and hyper-ramification of spinal microglia in CD-fed mice following PLX3397 treatment, further supporting the conception that microglia are highly dynamic cells and that consumption on a HFD alters spinal microglia morphology and functional responsibility to peripheral stimuli.

4.5. Limitations and future directions

First, PLX3397 was reportedly given by a mixture into a standard rodent diet or by gavage (Elmore et al., 2014; Wang et al., 2018), never be tried by intrathecal injection. Actually, PLX3397 was found to lead to the elimination of all microglia from the adult CNS (Elmore et al., 2014). Although PLX3397 likely depleted microglia in the brain regions such as hippocampus, cortex, and thalamus, there is no direct evidence for the role of microglia in these brain regions in pain modulation. However, it is becoming clear that microglia play an active role in these brain regions important for the emotional and memory-related aspects of chronic pain. We could not avoid the possible involvement of other regions of brain microglia in this model, but spinal microglia at least in part contribute to the exacerbated pain hypersensitivity, because selectively targeting of microglia by intrathecal injection of Mac-1-saporin in the spinal cord depleted microglia and attenuated both mechanical allodynia and thermal hyperalgesia in HFD-fed mice.

It is well known that microglia can secrete several pro-inflammatory and pro-nociceptive mediators such as TNF-α and BDNF to interact with neurons, thereby modulating synaptic transmission and pain states (Berta et al., 2014; Berta et al., 2016; Coull et al., 2005; Miyoshi et al., 2008). We observed in the present study that depletions of microglia inhibited TNF-α mRNA expression and BDNF release in the spinal cord, but we did not provide direct evidence of TNF-α and BDNF expression in spinal microglia.

Lastly, p38 MAPK is required for pain sensitization in male animals via microglial signaling (Berta et al., 2016; Luo et al., 2018; Taves et al., 2016), the transient depletion of microglia blocks allodynia in male mice but not in females (Sorge et al., 2015). In the present study, we aimed to perform the expression of p-p38 as a marker for microglial activation, did not design an experiment for further investigating the effects of a p38 inhibitor in pain responses in this model. It is also interesting to investigate PLX3397 and p38 inhibitor using female animals in this model.

In conclusion, this study provides multiple lines of evidence to show that HFD in mice induces long-lasting microglial reaction in the spinal cord, as characterized by hypertrophic cell morphology changes and increased p-p38 and CD16/32 expression. The neuroinflammatory reaction mediated by this reaction of spinal microglia increases the

expression of inflammatory cytokines like TNF-α and promotes the release of BDNF, thereby contributing to abnormal pain hypersensitivity in HFD-fed mice.

Acknowledgments

The image acquisition was supported by Biological Imaging and Analysis Laboratory, Medical and Healthy Analytical Center, Peking University, especially Qihua He, Jing Wu and Jiao Liu. This work was supported by the grants from the National Natural Science Foundation of China (81570997, 81870788, 81671085, 61527815) and the National Basic Research Program of China (973 Program, 2013CB531905).

Author contributions

YJL carried out the experiments, participated in the design of the study and drafted the manuscript. SYF, YPQ and KL performed experiments, analyzed the data and interpreted the results; ZRJ, HBJ and YJL participated in part of the behavioral test and provided assistance with data statistical analysis; JC provided assistance with reagents and techniques; GGX and KYF conceived and designed the study, revised the manuscript and made final approval of the version to be submitted. All authors have read and approved the final manuscript.

Competing interest

The authors declare no competing interest.

Appendix A. Supplementary data

Supplementary data to this article can be found online at https://doi.org/10.1016/j.bbi.2019.05.026.

References

Beggs, S., Trang, T., Salter, M.W., 2012. P2X4R+ microglia drive neuropathic pain. Nat. Neurosci. 15, 1068–1073.
Berta, T., Park, C.K., Xu, Z.Z., Xie, R.G., Liu, T., Lu, N., Liu, Y.C., Ji, R.R., 2014. Extracellular caspase-6 drives murine inflammatory pain via microglial TNF-alpha secretion. J. Clin. Invest. 124, 1173–1186.
Berta, T., Qadri, Y.J., Chen, G., Ji, R.R., 2016. Microglial signaling in chronic pain with a special focus on caspase 6, p38 MAP kinase, and sex dependence. J. Dent. Res. 95, 1124–1131.
Button, E.B., Mitchell, A.S., Domingos, M.M., Chung, J.H., Bradley, R.M., Hashemi, A., Marvyn, P.M., Patterson, A.C., Stark, K.D., Quadrilatero, J., Duncan, R.E., 2014. Microglial cell activation increases saturated and decreases monounsaturated fatty acid content, but both lipid species are proinflammatory. Lipids 49, 305–316.
Calvo, M., Bennett, D.L., 2012. The mechanisms of microgliosis and pain following peripheral nerve injury. Exp. Neurol. 234, 271–282.
Cawthorn, W.P., Sethi, J.K., 2008. TNF-alpha and adipocyte biology. FEBS Lett. 582, 117–131.
Chen, S.X., Wang, S.K., Yao, P.W., Liao, G.J., Na, X.D., Li, Y.Y., Zeng, W.A., Liu, X.G., Zang, Y., 2018. Early CALP2 expression and microglial activation are potential inducers of spinal IL-6 up-regulation and bilateral pain following motor nerve injury. J. Neurochem. 145, 154–169.
Cherry, J.D., Olschowka, J.A., O'Banion, M.K., 2014. Neuroinflammation and M2 microglia: the good, the bad, and the inflamed. J Neuroinflamm. 11, 98.
Colton, C.A., 2009. Heterogeneity of microglial activation in the innate immune response in the brain. J. Neuroimmun. Pharmacol. 4, 399–418.
Cooper, M.A., O'Meara, B., Jack, M.M., Elliot, D., Lamb, B., Khan, Z.W., Menta, B.W., Ryals, J.M., Winter, M.K., Wright, D.E., 2018. Intrinsic activity of C57BL/6 substrains associates with high-fat diet-induced mechanical sensitivity in mice. J. Pain 19 (11), 1285–1295.
Cooper, M.A., Ryals, J.M., Wu, P.Y., Wright, K.D., Walter, K.R., Wright, D.E., 2017. Modulation of diet-induced mechanical allodynia by metabolic parameters and inflammation. J. Peripher. Nerv. Syst. 22, 39–46.
Coull, J.A., Beggs, S., Boudreau, D., Boivin, D., Tsuda, M., Inoue, K., Gravel, C., Salter, M.W., De Koninck, Y., 2005. BDNF from microglia causes the shift in neuronal anion gradient underlying neuropathic pain. Nature 438, 1017–1021.
da Cruz Fernandes, I.M., Pinto, R.Z., Ferreira, P., Lira, F.S., 2018. Low back pain, obesity, and inflammatory markers: exercise as potential treatment. J. Exerc. Rehabil. 14, 168–174.
de Kloet, A.D., Pioquinto, D.J., Nguyen, D., Wang, L., Smith, J.A., Hiller, H., Sumners, C., 2014. Obesity induces neuroinflammation mediated by altered expression of the renin-angiotensin system in mouse forebrain nuclei. Physiol. Behav. 136, 31–38.
Echeverry, S., Shi, X.Q., Yang, M., Huang, H., Wu, Y., Lorenzo, L.E., Perez-Sanchez, J., Bonin, R.P., De Koninck, Y., Zhang, J., 2017. Spinal microglia are required for long-term maintenance of neuropathic pain. Pain 158, 1792–1801.
Echeverry, S., Shi, X.Q., Zhang, J., 2008. Characterization of cell proliferation in rat spinal cord following peripheral nerve injury and the relationship with neuropathic pain. Pain 135, 37–47.
Elmore, M.R., Najafi, A.R., Koike, M.A., Dagher, N.N., Spangenberg, E.E., Rice, R.A., Kitazawa, M., Matusow, B., Nguyen, H., West, B.L., Green, K.N., 2014. Colony-stimulating factor 1 receptor signaling is necessary for microglia viability, unmasking a microglia progenitor cell in the adult brain. Neuron 82, 380–397.
Erblich, B., Zhu, L., Etgen, A.M., Dobrenis, K., Pollard, J.W., 2011. Absence of colony stimulation factor-1 receptor results in loss of microglia, disrupted brain development and olfactory deficits. PLoS One 6, e26317.
Erny, D., Hrabe de Angelis, A.L., Jaitin, D., Wieghofer, P., Staszewski, O., David, E., Keren-Shaul, H., Mahlakoiv, T., 2015. Host microbiota constantly control maturation and function of microglia in the CNS. Nat. Neurosci. 18, 965–977.
Fang, D., Kong, L.Y., Cai, J., Li, S., Liu, X.D., Han, J.S., Xing, G.G., 2015. Interleukin-6-mediated functional upregulation of TRPV1 receptors in dorsal root ganglion neurons through the activation of JAK/PI3K signaling pathway: roles in the development of bone cancer pain in a rat model. Pain 156, 1124–1144.
Ferrini, F., Trang, T., Mattioli, T.A., Laffray, S., Del'Guidice, T., Lorenzo, L.E., Castonguay, A., Doyon, N., Zhang, W., Godin, A.G., Mohr, D., Beggs, S., Vandal, K., Beaulieu, J.M., Cahill, C.M., Salter, M.W., De Koninck, Y., 2013. Morphine hyperalgesia gated through microglia-mediated disruption of neuronal Cl(-) homeostasis. Nat. Neurosci. 16, 183–192.
Galante, M., Jani, H., Vanes, L., Daniel, H., Fisher, E.M., Tybulewicz, V.L., Bliss, T.V., Morice, E., 2009. Impairments in motor coordination without major changes in cerebellar plasticity in the Tc1 mouse model of Down syndrome. Hum. Mol. Genet. 18, 1449–1463.
Goings, G.E., Kozlowski, D.A., Szele, F.G., 2006. Differential activation of microglia in neurogenic versus non-neurogenic regions of the forebrain. Glia 54, 329–342.
Grace, P.M., Hutchinson, M.R., Maier, S.F., Watkins, L.R., 2014. Pathological pain and the neuroimmune interface. Nat. Rev. Immunol. 14, 217–231.
Gregor, M.F., Hotamisligil, G.S., 2011. Inflammatory mechanisms in obesity. Annu. Rev. Immunol. 29, 415–445.
Guan, Z., Kuhn, J.A., Wang, X., Colquitt, B., Solorzano, C., Vaman, S., Guan, A.K., Evans-Reinsch, Z., Braz, J., Devor, M., Abboud-Werner, S.L., Lanier, L.L., 2016. Injured sensory neuron-derived CSF1 induces microglial proliferation and DAP12-dependent pain. Nat. Neurosci. 19, 94–101.
Guillemot-Legris, O., Buisseret, B., Mutemberezi, V., Hermans, E., Deumens, R., Alhouayek, M., Muccioli, G.G., 2018. Post-operative pain in mice is prolonged by diet-induced obesity and rescued by dietary intervention. Brain Behav. Immun. 74, 96–105.
Guillemot-Legris, O., Muccioli, G.G., 2017. Obesity-induced neuroinflammation: beyond the hypothalamus. Trends Neurosci. 40, 237–253.
Hanisch, U.K., 2013. Functional diversity of microglia – how heterogeneous are they to begin with? Front. Cell. Neurosci. 7, 65.
Hanisch, U.K., Kettenmann, H., 2007. Microglia: active sensor and versatile effector cells in the normal and pathologic brain. Nat. Neurosci. 10, 1387–1394.
Hao, S., Dey, A., Yu, X., Stranahan, A.M., 2016. Dietary obesity reversibly induces synaptic stripping by microglia and impairs hippocampal plasticity. Brain Behav. Immun. 51, 230–239.
Heim, N., Snijder, M.B., Deeg, D.J., Seidell, J.C., Visser, M., 2008. Obesity in older adults is associated with an increased prevalence and incidence of pain. Obesity (Silver Spring) 16, 2510–2517.
Hellwig, S., Brioschi, S., Dieni, S., Frings, L., Masuch, A., Blank, T., Biber, K., 2016. Altered microglia morphology and higher resilience to stress-induced depression-like behavior in CX3CR1-deficient mice. Brain Behav. Immun. 55, 126–137.
Hellwig, S., Heinrich, A., Biber, K., 2013. The brain's best friend: microglial neurotoxicity revisited. Front. Cell. Neurosci. 7, 71.
Hitt, H.C., McMillen, R.C., Thornton-Neaves, T., Koch, K., Cosby, A.G., 2007. Comorbidity of obesity and pain in a general population: results from the Southern Pain Prevalence Study. J. Pain 8, 430–436.
Hu, X., Li, P., Guo, Y., Wang, H., Leak, R.K., Chen, S., Gao, Y., Chen, J., 2012. Microglia/macrophage polarization dynamics reveal novel mechanism of injury expansion after focal cerebral ischemia. Stroke 43, 3063–3070.
Ji, R.R., Berta, T., Nedergaard, M., 2013. Glia and pain: is chronic pain a gliopathy? Pain 154 (Suppl 1), S10–28.
Ji, R.R., Suter, M.R., 2007. p38 MAPK, microglial signaling, and neuropathic pain. Mol. Pain 3, 33.
Kawasaki, Y., Zhang, L., Cheng, J.K., Ji, R.R., 2008. Cytokine mechanisms of central sensitization: distinct and overlapping role of interleukin-1beta, interleukin-6, and tumor necrosis factor-alpha in regulating synaptic and neuronal activity in the superficial spinal cord. J. Neurosci. : Off. J. Soc. Neurosci. 28, 5189–5194.
Keane, D., Kelly, S., Healy, N.P., McArdle, M.A., Holohan, K., Roche, H.M., 2013. Diet and metabolic syndrome: an overview. Curr. Vasc. Pharmacol. 11, 842–857.
Kennedy, A., Martinez, K., Chuang, C.C., LaPoint, K., McIntosh, M., 2009. Saturated fatty acid-mediated inflammation and insulin resistance in adipose tissue: mechanisms of action and implications. J. Nutr. 139, 1–4.
Kettenmann, H., Hanisch, U.K., Noda, M., Verkhratsky, A., 2011. Physiology of microglia. Physiol. Rev. 91, 461–553.
Li, K., Lin, T., Cao, Y., Light, A.R., Fu, K.Y., 2010. Peripheral formalin injury induces 2 stages of microglial activation in the spinal cord. J. Pain 11, 1056–1065.
Liddelow, S.A., Guttenplan, K.A., Clarke, L.E., Bennett, F.C., Bohlen, C.J., Schirmer, L., Bennett, M.L., Munch, A.E., Chung, W.S., Peterson, T.C., Wilton, D.K., Frouin, A.,

Napier, B.A., Panicker, N., Kumar, M., Buckwalter, M.S., Rowitch, D.H., Dawson, V.L., Dawson, T.M., Stevens, B., Barres, B.A., 2017. Neurotoxic reactive astrocytes are induced by activated microglia. Nature 541, 481–487.
London, A., Cohen, M., Schwartz, M., 2013. Microglia and monocyte-derived macrophages: functionally distinct populations that act in concert in CNS plasticity and repair. Front. Cell. Neurosci. 7, 34.
Loredo-Perez, A.A., Montalvo-Blanco, C.E., Hernandez-Gonzalez, L.I., Anaya-Reyes, M., Fernandez Del Valle-Laisequilla, C., Reyes-Garcia, J.G., Acosta-Gonzalez, R.I., Martinez-Martinez, A., Villarreal-Salcido, J.C., Vargas-Munoz, V.M., Munoz-Islas, E., Ramirez-Rosas, M.B., Jimenez-Andrade, J.M., 2016. High-fat diet exacerbates pain-like behaviors and periarticular bone loss in mice with CFA-induced knee arthritis. Obesity (Silver Spring) 24, 1106–1115.
Luo, X., Fitzsimmons, B., Mohan, A., Zhang, L., Terrando, N., Kordasiewicz, H., Ji, R.R., 2018. Intrathecal administration of antisense oligonucleotide against p38alpha but not p38beta MAP kinase isoform reduces neuropathic and postoperative pain and TLR4-induced pain in male mice. Brain Behav. Immun. 72, 34–44.
Marcus, D.A., 2004. Obesity and the impact of chronic pain. Clin. J. Pain 20, 186–191.
McCarthy, L.H., Bigal, M.E., Katz, M., Derby, C., Lipton, R.B., 2009. Chronic pain and obesity in elderly people: results from the Einstein aging study. J. Am. Geriatr. Soc. 57, 115–119.
McMahon, S.B., Malcangio, M., 2009. Current challenges in glia-pain biology. Neuron 64, 46–54.
Miyoshi, K., Obata, K., Kondo, T., Okamura, H., Noguchi, K., 2008. Interleukin-18-mediated microglia/astrocyte interaction in the spinal cord enhances neuropathic pain processing after nerve injury. J. Neurosci: Off. J. Soc. Neurosci. 28, 12775–12787.
Mok, S., Koya, R.C., Tsui, C., Xu, J., Robert, L., Wu, L., Graeber, T., West, B.L., Bollag, G., Ribas, A., 2014. Inhibition of CSF-1 receptor improves the antitumor efficacy of adoptive cell transfer immunotherapy. Cancer Res. 74, 153–161.
Nadjar, A., Leyrolle, Q., Joffre, C., Laye, S., 2017. Bioactive lipids as new class of microglial modulators: when nutrition meets neuroimunology. Prog. Neuro-Psychopharmacol. Biol. Psychiatry 79, 19–26.
Nandi, S., Gokhan, S., Dai, X.M., Wei, S., Enikolopov, G., Lin, H., Mehler, M.F., Stanley, E.R., 2012. The CSF-1 receptor ligands IL-34 and CSF-1 exhibit distinct developmental brain expression patterns and regulate neural progenitor cell maintenance and maturation. Dev. Biol. 367, 100–113.
Narouze, S., Souzdalnitski, D., 2015. Obesity and chronic pain: systematic review of prevalence and implications for pain practice. Reg. Anesth. Pain Med. 40, 91–111.
Old, E.A., Malcangio, M., 2012. Chemokine mediated neuron-glia communication and aberrant signalling in neuropathic pain states. Curr. Opin. Pharmacol. 12, 67–73.
Paulis, W.D., Silva, S., Koes, B.W., van Middelkoop, M., 2014. Overweight and obesity are associated with musculoskeletal complaints as early as childhood: a systematic review. Obes. Rev. 15, 52–67.
Plomgaard, P., Nielsen, A.R., Fischer, C.P., Mortensen, O.H., Broholm, C., Penkowa, M., Krogh-Madsen, R., Erikstrup, C., Lindegaard, B., Petersen, A.M., Taudorf, S., Pedersen, B.K., 2007. Associations between insulin resistance and TNF-alpha in plasma, skeletal muscle and adipose tissue in humans with and without type 2 diabetes. Diabetologia 50, 2562–2571.
Pogatzki, E.M., Raja, S.N., 2003. A mouse model of incisional pain. Anesthesiology 99, 1023–1027.
Ransohoff, R.M., 2016. A polarizing question: do M1 and M2 microglia exist? Nat. Neurosci. 19, 987–991.
Rosen, S.F., Ham, B., Haichin, M., Walters, I.C., Tohyama, S., Sotocinal, S.G., Mogil, J.S., 2019. Increased pain sensitivity and decreased opioid analgesia in T-cell-deficient mice and implications for sex differences. Pain 160, 358–366.
Rossi, H.L., Broadhurst, K.A., Luu, A.S., Lara, O., Kothari, S.D., Mohapatra, D.P., Recober, A., 2016. Abnormal trigeminal sensory processing in obese mice. Pain 157, 235–246.
Rossi, H.L., Luu, A.K., DeVilbiss, J.L., Recober, A., 2013. Obesity increases nociceptive activation of the trigeminal system. Eur. J. Pain 17, 649–653.
Sampson, T.R., Debelius, J.W., Thron, T., Janssen, S., Shastri, G.G., Ilhan, Z.E., Challis, C., Schretter, C.E., Rocha, S., Gradinaru, V., Chesselet, M.F., Keshavarzian, A., Shannon, K.M., Krajmalnik-Brown, R., Wittung-Stafshede, P., Knight, R., Mazmanian, S.K., 2016. Gut microbiota regulate motor deficits and neuroinflammation in a model of Parkinson's disease. Cell 167, 1469–1480.e1412.
Sawada, A., Niiyama, Y., Ataka, K., Nagaishi, K., Yamakage, M., Fujimiya, M., 2014. Suppression of bone marrow-derived microglia in the amygdala improves anxiety-like behavior induced by chronic partial sciatic nerve ligation in mice. Pain 155, 1762–1772.
Schistad, E.I., Stubhaug, A., Furberg, A.S., Engdahl, B.L., Nielsen, C.S., 2017. C-reactive protein and cold-pressor tolerance in the general population: the Tromso Study. Pain 158, 1280–1288.
Schreyer, S.A., Chua Jr., S.C., LeBoeuf, R.C., 1998. Obesity and diabetes in TNF-alpha receptor- deficient mice. J. Clin. Invest. 102, 402–411.
Sibille, K.T., Steingrimsdottir, O.A., Fillingim, R.B., Stubhaug, A., Schirmer, H., Chen, H., McEwen, B.S., Nielsen, C.S., 2016. Investigating the burden of chronic pain: an inflammatory and metabolic composite. Pain Res. Manage. 2016, 7657329.
Smuck, M., Kao, M.C., Brar, N., Martinez-Ith, A., Choi, J., Tomkins-Lane, C.C., 2014. Does physical activity influence the relationship between low back pain and obesity? Spine J. 14, 209–216.
Song, Z., Xie, W., Chen, S., Strong, J.A., Print, M.S., Wang, J.I., Shareef, A.F., Ulrich-Lai, Y.M., Zhang, J.M., 2017. High-fat diet increases pain behaviors in rats with or without obesity. Sci. Rep. 7, 10350.
Song, Z., Xie, W., Strong, J.A., Berta, T., Ulrich-Lai, Y.M., Guo, Q., Zhang, J.M., 2018. High-fat diet exacerbates postoperative pain and inflammation in a sex-dependent manner. Pain 159, 1731–1741.
Sorge, R.E., Mapplebeck, J.C., Rosen, S., Beggs, S., Taves, S., Alexander, J.K., Martin, L.J., Austin, J.S., Sotocinal, S.G., Chen, D., Yang, M., Shi, X.Q., Huang, H., Pillon, N.J., Bilan, P.J., Tu, Y., Klip, A., Ji, R.R., Zhang, J., Salter, M.W., 2015. Different immune cells mediate mechanical pain hypersensitivity in male and female mice. Nat. Neurosci. 18, 1081–1083.
Stone, A.A., Broderick, J.E., 2012. Obesity and pain are associated in the United States. Obesity (Silver Spring) 20, 1491–1495.
Taves, S., Berta, T., Liu, D.L., Gan, S., Chen, G., Kim, Y.H., Van de Ven, T., Laufer, S., Ji, R.R., 2016. Spinal inhibition of p38 MAP kinase reduces inflammatory and neuropathic pain in male but not female mice: sex-dependent microglial signaling in the spinal cord. Brain Behav. Immun. 55, 70–81.
Taylor, P.R., Martinez-Pomares, L., Stacey, M., Lin, H.H., Brown, G.D., Gordon, S., 2005. Macrophage receptors and immune recognition. Annu. Rev. Immunol. 23, 901–944.
Thaler, J.P., Guyenet, S.J., Dorfman, M.D., Wisse, B.E., Schwartz, M.W., 2013. Hypothalamic inflammation: marker or mechanism of obesity pathogenesis? Diabetes 62, 2629–2634.
Trang, T., Beggs, S., Salter, M.W., 2012. ATP receptors gate microglia signaling in neuropathic pain. Exp. Neurol. 234, 354–361.
Trang, T., Beggs, S., Wan, X., Salter, M.W., 2009. P2X4-receptor-mediated synthesis and release of brain-derived neurotrophic factor in microglia is dependent on calcium and p38-mitogen-activated protein kinase activation. J. Neurosci.: Off. J. Soc. Neurosci. 29, 3518–3528.
Tsuda, M., Beggs, S., Salter, M.W., Inoue, K., 2013. Microglia and intractable chronic pain. Glia 61, 55–61.
Tzanavari, T., Giannogonas, P., Karalis, K.P., 2010. TNF-alpha and obesity. Curr. Dir. Autoimmun. 11, 145–156.
Ueda, H., Neyama, H., Nagai, J., Matsushita, Y., Tsukahara, T., Tsukahara, R., 2018. Involvement of lysophosphatidic acid-induced astrocyte activation underlying the maintenance of partial sciatic nerve injury-induced neuropathic pain. Pain 159, 2170–2178.
Valdearcos, M., Douglass, J.D., Robblee, M.M., Dorfman, M.D., Stifler, D.R., Bennett, M.L., Gerritse, I., Fasnacht, R., Barres, B.A., Thaler, J.P., Koliwad, S.K., 2017. Microglial inflammatory signaling orchestrates the hypothalamic immune response to dietary excess and mediates obesity susceptibility. Cell Metab. 26, 185–197.e183.
Valdearcos, M., Robblee, M.M., Benjamin, D.I., Nomura, D.K., Xu, A.W., Koliwad, S.K., 2014. Microglia dictate the impact of saturated fat consumption on hypothalamic inflammation and neuronal function. Cell Rep. 9, 2124–2138.
Valdearcos, M., Xu, A.W., Koliwad, S.K., 2015. Hypothalamic inflammation in the control of metabolic function. Annu. Rev. Physiol. 77, 131–160.
Valerio, A., Cardile, A., Cozzi, V., Bracale, R., Tedesco, L., Pisconti, A., Palomba, L., Cantoni, O., Clementi, E., Moncada, S., Carruba, M.O., Nisoli, E., 2006. TNF-alpha downregulates eNOS expression and mitochondrial biogenesis in fat and muscle of obese rodents. J. Clin. Invest. 116, 2791–2798.
Wang, G.Y.F., Shi, X.Q., Wu, W., Gueorguieva, M., Yang, M., Zhang, J., 2018. Sustained and repeated mouth opening leads to development of painful temporomandibular disorders involving macrophage/microglia activation in mice. Pain 159, 1277–1288.
Wang, N., Liang, H., Zen, K., 2014. Molecular mechanisms that influence the macrophage m1–m2 polarization balance. Front. Immunol. 5, 614.
Wang, Z., Liu, D., Wang, F., Liu, S., Zhao, S., Ling, E.A., Hao, A., 2012. Saturated fatty acids activate microglia via Toll-like receptor 4/NF-kappaB signalling. Br. J. Nutr. 107, 229–241.
Yao, Y., Echeverry, S., Shi, X.Q., Yang, M., Yang, Q.Z., Wang, G.Y., Chambon, J., Wu, Y.C., Fu, K.Y., De Koninck, Y., Zhang, J., 2016. Dynamics of spinal microglia repopulation following an acute depletion. Sci. Rep. 6, 22839.
Zhang, J., De Koninck, Y., 2006. Spatial and temporal relationship between monocyte chemoattractant protein-1 expression and spinal glial activation following peripheral nerve injury. J. Neurochem. 97, 772–783.
Zhang, J., Echeverry, S., Lim, T.K., Lee, S.H., Shi, X.Q., Huang, H., 2015. Can modulating inflammatory response be a good strategy to treat neuropathic pain? Curr. Pharm. Des. 21, 831–839.
Zhang, J., Shi, X.Q., Echeverry, S., Mogil, J.S., De Koninck, Y., Rivest, S., 2007. Expression of CCR2 in both resident and bone marrow-derived microglia plays a critical role in neuropathic pain. J. Neurosci.: Off. J. Soc. Neurosci. 27, 12396–12406.
Zhao, P., Waxman, S.G., Hains, B.C., 2007. Extracellular signal-regulated kinase-regulated microglia-neuron signaling by prostaglandin E2 contributes to pain after spinal cord injury. J. Neurosci.: Off. J. Soc. Neurosci. 27, 2357–2368.
Zhuang, Z.Y., Gerner, P., Woolf, C.J., Ji, R.R., 2005. ERK is sequentially activated in neurons, microglia, and astrocytes by spinal nerve ligation and contributes to mechanical allodynia in this neuropathic pain model. Pain 114, 149–159.